Activities of the Val Space Consortium and the European Space Agency in the Study of RF Breakdown Phenomena in Microwave Passive Components for Space Applications

Benito Gimeno[1,3], Vicente E. Boria[2,3], David Argilés[3], David Raboso[4]

(1) University of Valencia, Spain

(2) Technical University of Valencia, Spain

(3) VAL SPACE CONSORTIUM, Valencia, Spain

(4) European Space Agency, ESA/ESTEC, The Netherlands

ECLOUD'12

5-9 June 2012, La Biodola, Isola d'Elba, Italy

EL CONSORCIO ESPACIAL VALENCIANO ESTÁ INTEGRADO POR / VAL SPACECONSORTIUM IS COMPOSED BY:

UNIVERSIDAD POLITECNICA DE VALENCIA | GENERALITAT VALENCIANA | AJUNTAMENT DE VALENCIA | VNIVERSITAT DE VALÈNCIA

INDEX

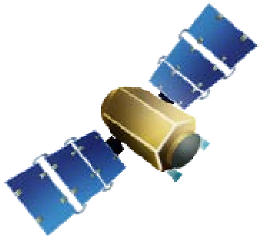

- Introduction
- VAL SPACE CONSORTIUM presentation
- European High Power RF Space Laboratory
- European High Power Space Materials Laboratory
- R&D activities
- Conclusions

INDEX

- Introduction
- VAL SPACE CONSORTIUM presentation
- European High Power RF Space Laboratory
- European High Power Space Materials Laboratory
- R&D activities
- Conclusions

Introduction

- Space weather is a very hostile environment
- Solar activity causes a continuous flux of high energy elemental particles towards the spaceships

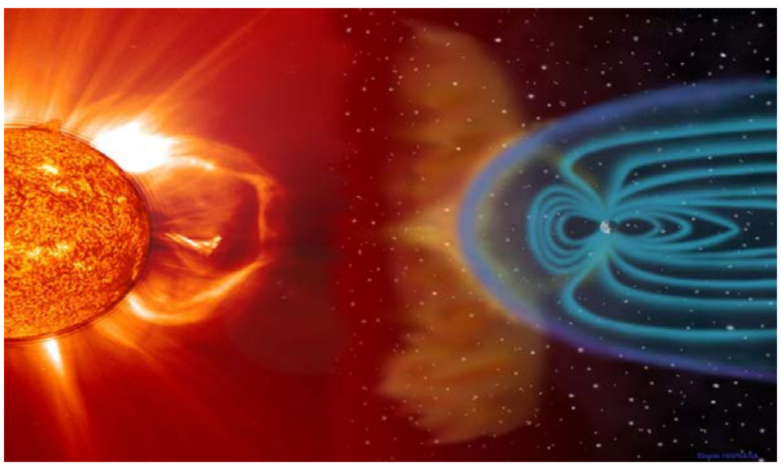

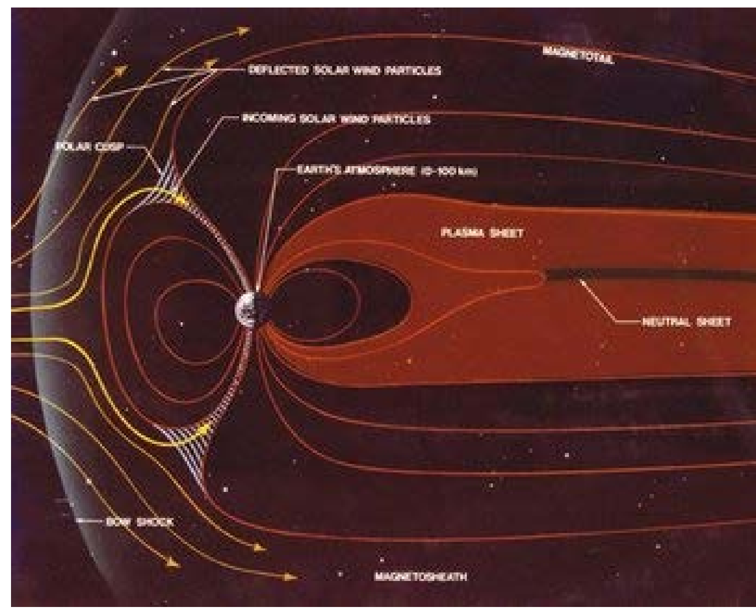

Introduction

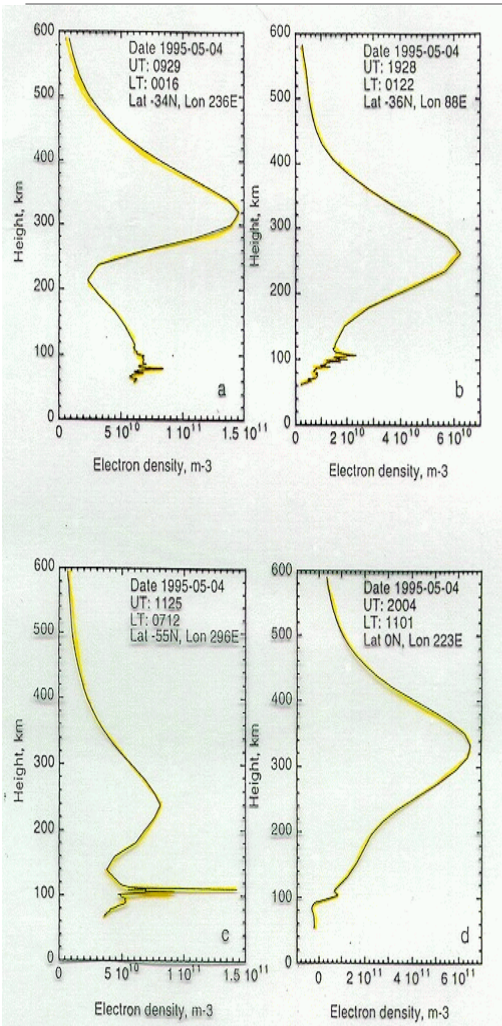

- Electron density versus heigth (related to Earth surface) for different Earth points demonstrates a very high population of electrons around 300 km
- In a satellite: Cosmic radiation, Sun (fotoelectric effect), and Van Allen rings (1000-5000 km)

Initial electron density requested for a multipactor discharge in a Ku band component:
$\rho \sim 5\ 10^{10}$ electrones/m^3

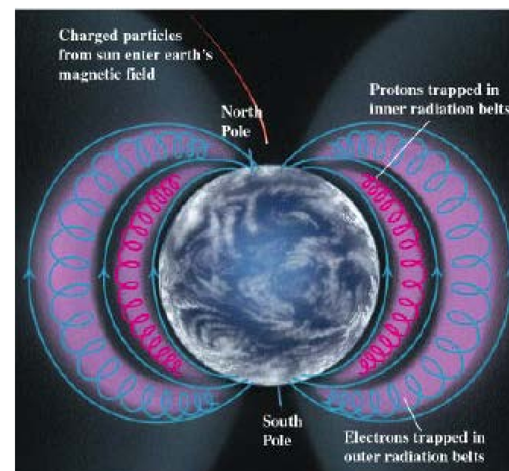

- **Multipactor effect**: electrons avalanche generated by the synchonization between an intense RF electric field and the secondary electron emission phenomenon (SEEY) under ultra high-vacuum conditions

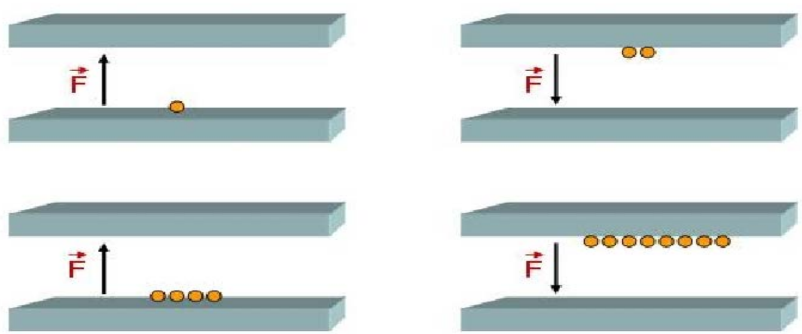

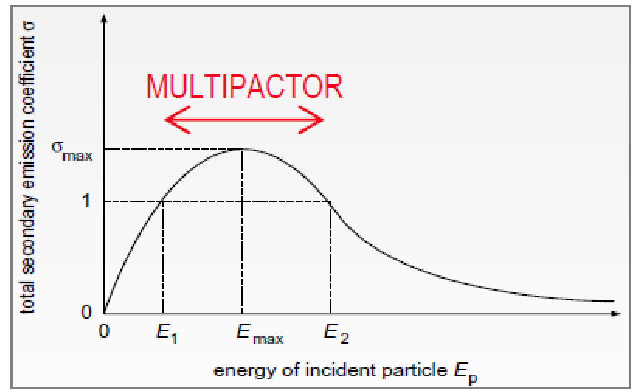

- Multipactor effect migth occur mainly in:

  - RF satellite components

  - Particle accelerators structures

- In these systems produces: noise, increase of the reflection coefficient, local surface heating, detuning electrical circuit, surface damage and possible breakdown of the component

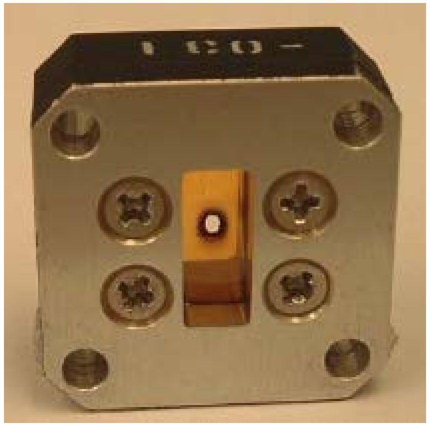

Kapton window

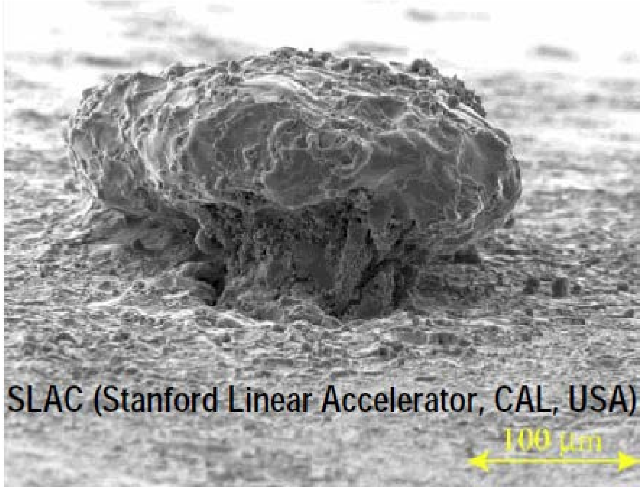

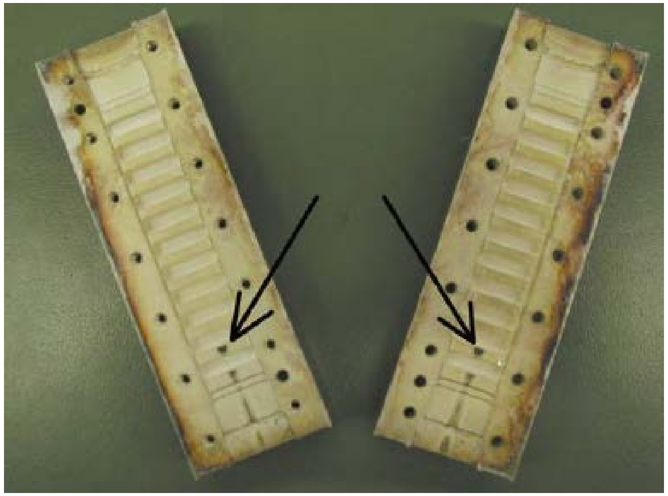

Low-pass filter

- In this undesired scenario the space agencies have to control and predict the possible existence of a multipactor discharge occurring within on-board microwave sub-systems: **replacement of equipments is NOT POSSIBLE in a satellite …**

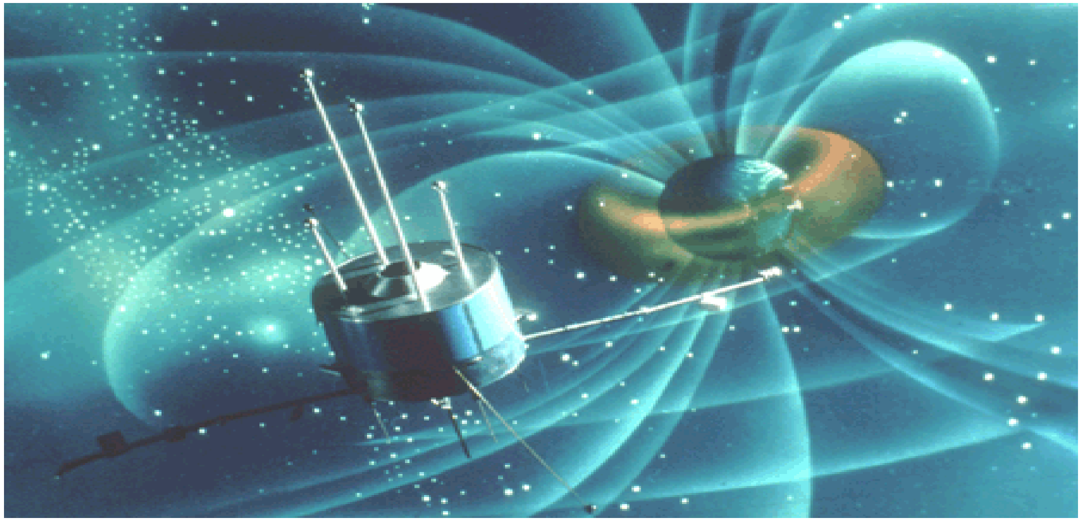

INDEX

VAL SPACE CONSORTIUM presentation

- Val Space Consortium (VSC) is a public consortium
- Non-profit organization
- It is focused on providing testing services, consultancy, training and development of R&D activities in the Space field

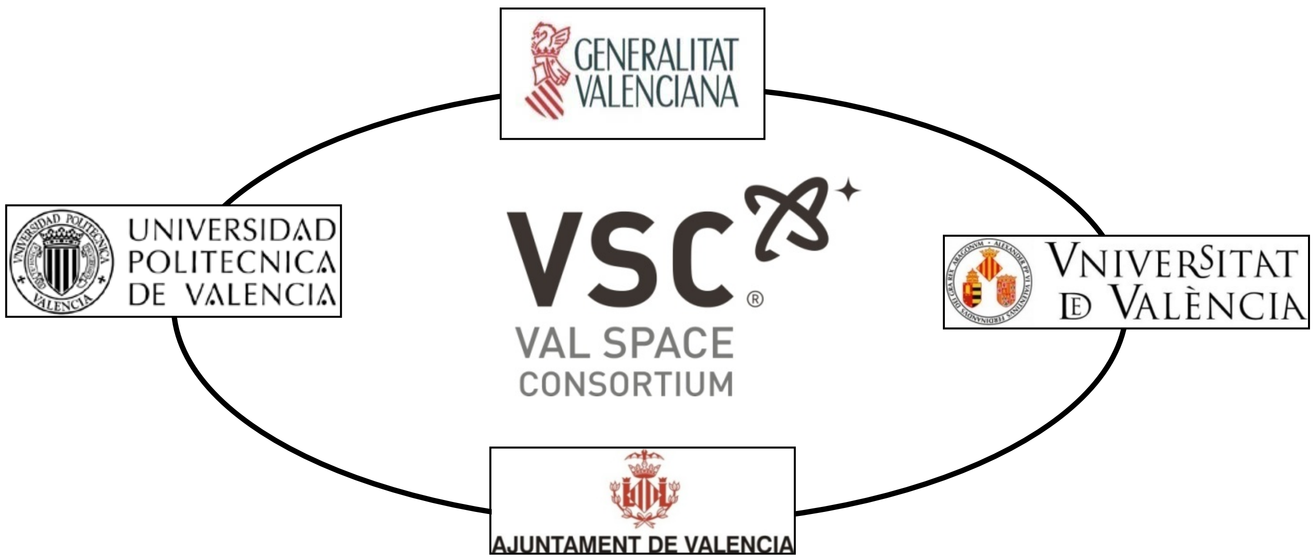

- On 25 March 2010, ESA and VSC signed a contract to jointly manage the European High Power RF Space Laboratory.

- The **contract signature** followed an announcement of opportunity issued during the summer of 2009 by ESA in search of a partner to provide competence and facilities to support to the operation, maintenance and development of the Laboratory.
- Among the proposals received, **VSC was selected**.
- ESA continues as the single **interface** for space-related testing activities.

- Human Resources: Laboratory structure

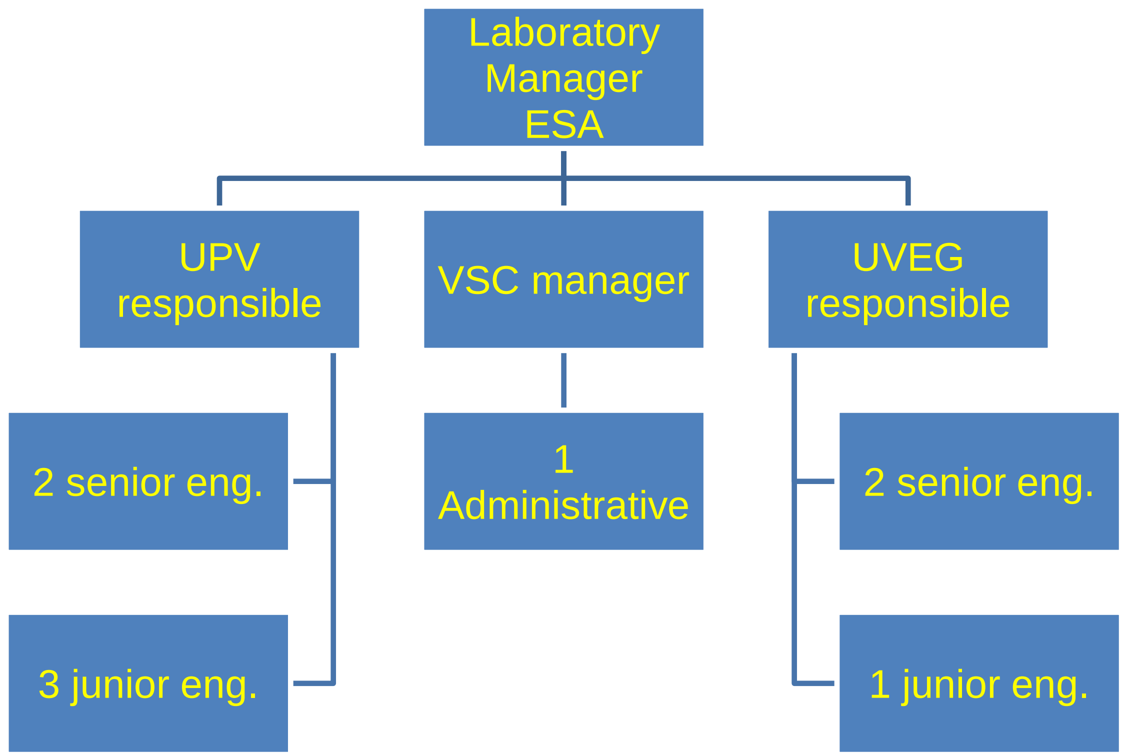

INDEX

- Introduction
- VAL SPACE CONSORTIUM presentation
- European High Power RF Space Laboratory
- European High Power Space Materials Laboratory
- R&D activities
- Conclusions

European High Power RF Space Laboratory

- Opening of the Laboratory: 28 June 2010.

- Technical Resources
  - Test beds from 400 MHz to 40 GHz
  - Around 30 RF power amplifiers (CW and pulsed)
  - Waveguide (rectangular and circular), coaxial and microstrip
  - Vector network analyzers, Spectrum analyzers, Oscilloscopes, etc …

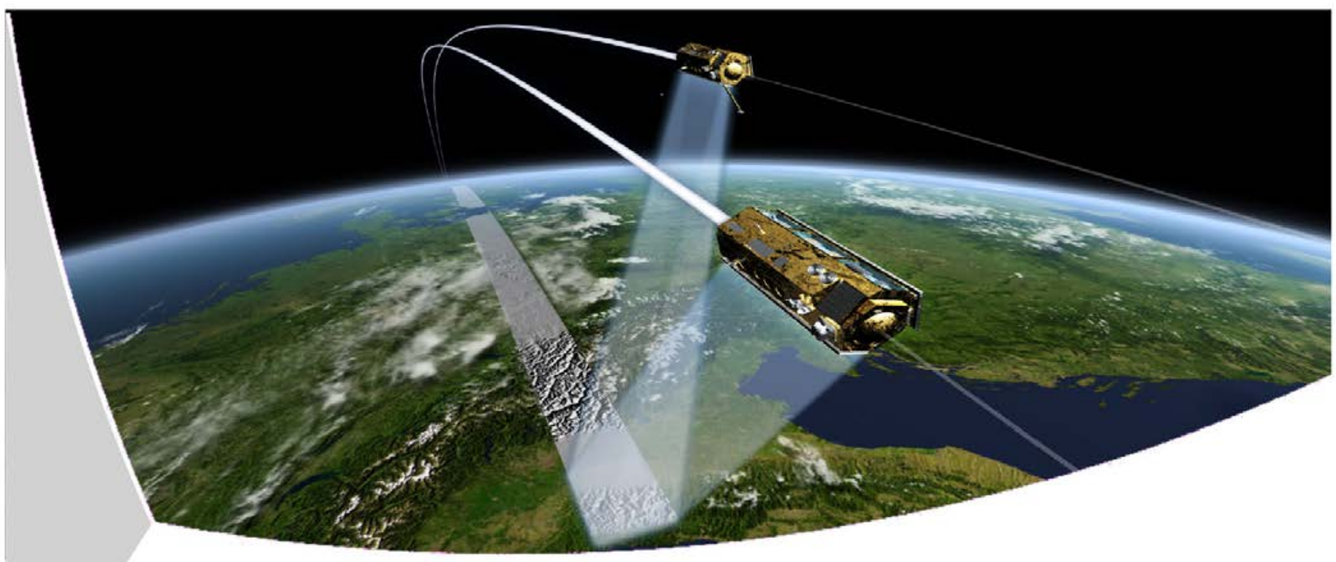

- Up to date the Laboratory can carry out these **tests**:
  - Multipactor effect: Single-carrier and Multicarrier
  - Corona effect
  - Power Handling
  - Passive Intermodulation (PIM): guided and radiated
- Next, the **facilities** of the Laboratory are presented.

- Installed in the *Innovation Polytechnic City* (Technical University of Valencia):

- Clean room 1 (150m^2) – Class 10,000

- Clean room 2 ($50m^2$) – Class 10,000

- Vacuum system 1

Chamber Dimensions	
Diameter	1200 mm
Depth	2700 mm

Base Plate Dimensions	
Length	120 mm
Width	345 mm

Pressure Range	
Maximum	1000 mbar
Minimum	10^{-6} mbar

Temperature Range
Not available

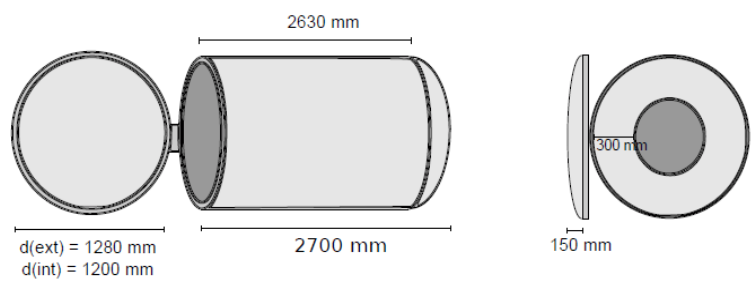

- Vacuum system 2

Chamber Dimensions		Base Plate Dimensions	
Diameter	595 mm	Diameter	480 mm
Depth	360 mm		

Pressure Range		Temperature Range	
Maximum	1000 mbar	Maximum	+140°
Minimum	10^{-7} mbar	Minimum	−40°

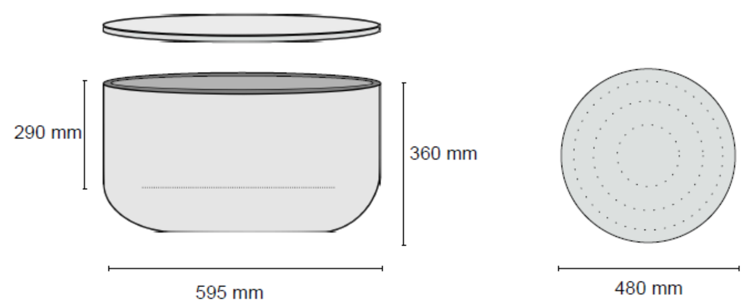

European High Power RF Space Laboratory

- Vacuum system 3

Chamber Dimensions		Base Plate Dimensions	
Diameter	595 mm	Length	650 mm
Depth	940 mm	Width	420 mm

Pressure Range		Temperature Range	
Maximum	1000 mbar	Maximum	$+130°$
Minimum	10^{-8} mbar	Minimum	$-65°$

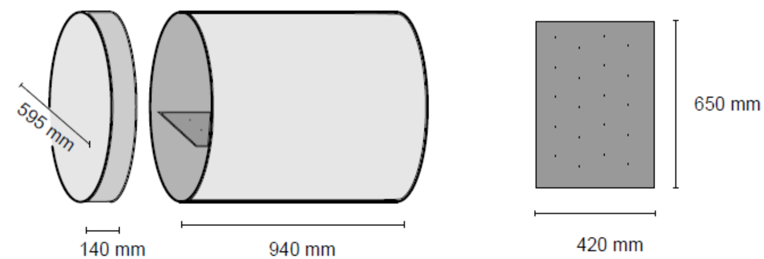

Pressure profile of Arian-5 rocket:

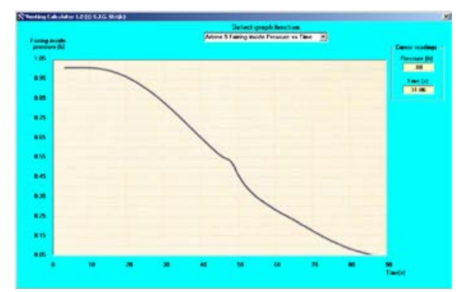

- Vacuum system 4

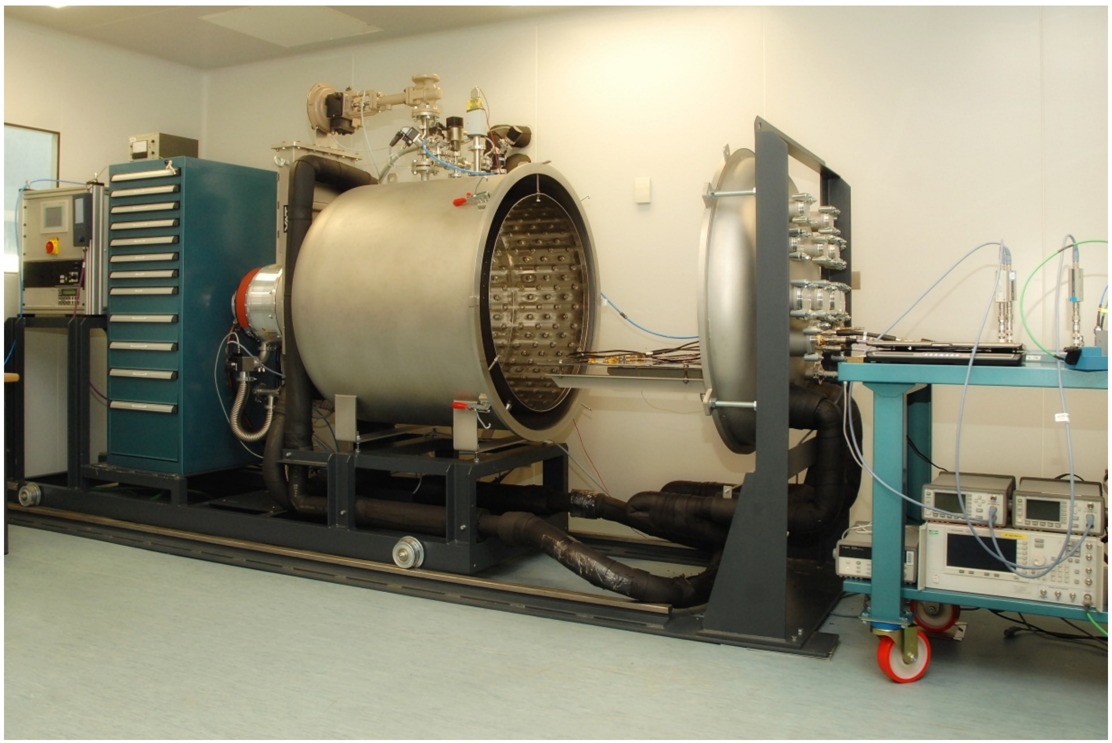

Chamber Dimensions		Base Plate Dimensions	
Diameter	830 mm	Length	640 mm
Depth	730 mm	Width	640 mm

Pressure Range		Temperature Range	
Maximum	1000 mbar	Maximum	+120°
Minimum	10^{-7} mbar	Minimum	−70°

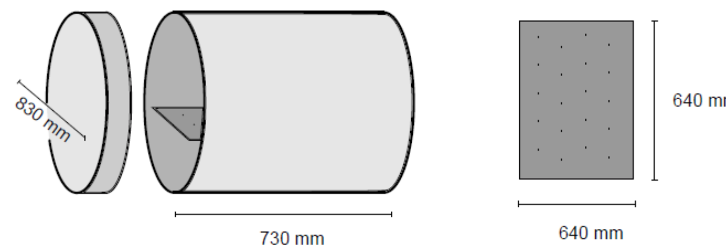

- Vacuum system 5

Chamber Dimensions		Base Plate Dimensions
Diameter	295 mm	Not available
Depth	450 mm	

Pressure Range		Temperature Range
Maximum	1000 mbar	Not available
Minimum	10^{-6} mbar	

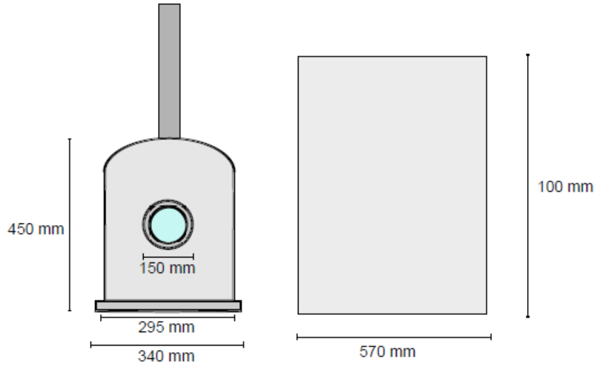

European High Power RF Space Laboratory

- Anechoic chamber: PIM radiated

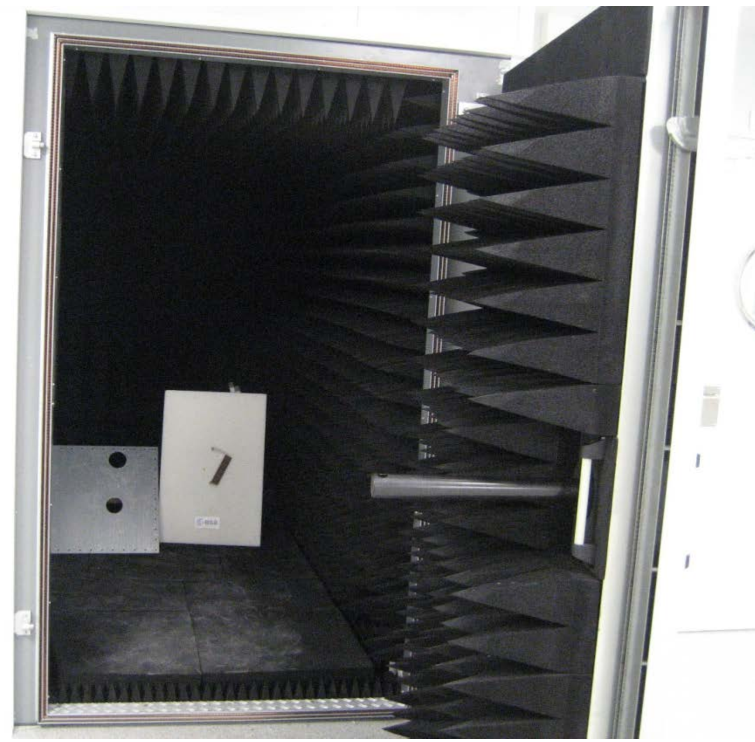

European High Power RF Space Laboratory

- Dielectric radome for PIM measurements of antennas and radiating elements (10^{-6} mbar)

- Multipactor-Multicarrier facility
  - 10 carriers of 400 watts each
  - Water cooled system
  - Fully automatic by software
  - Flexible and modular
  - State-of-the-art system
  - Unique in the World
  - Ku-band

INDEX

- Introduction
- VAL SPACE CONSORTIUM presentation
- European High Power RF Space Laboratory
- European High Power Space Materials Laboratory
- R&D activities
- Conclusions

- Installed in the *Technical School of Engineering* (University of Valencia):

Inauguration:

9th July 2012

- X-Ray/Ultraviolet Photoelectron Spectroscopy (XPS/UPS)

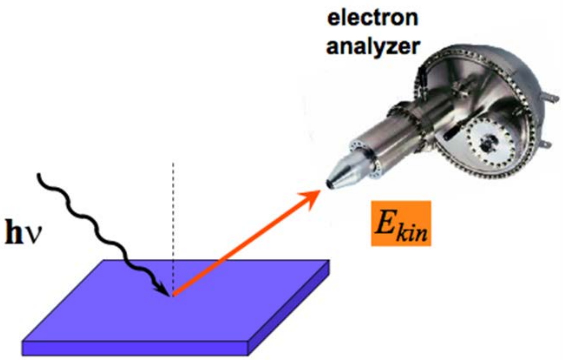

Ultra high-vacuum

(10^{-9} mbar)

Measurement of SEEY for both metals and dielectric materials

- Evaporation systems in high-vacuum (10^{-6} mbar)

Sputtering technique for low-SEEY multilayers growthing

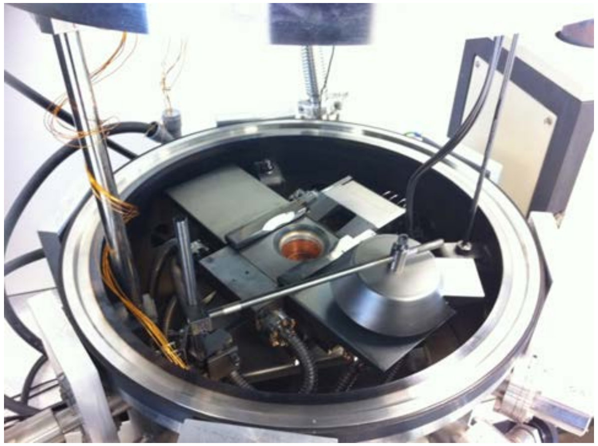

- Vacuum chamber for measurements of venting and outgassing phenomena (10^{-5} mbar) with a mass spectrometer

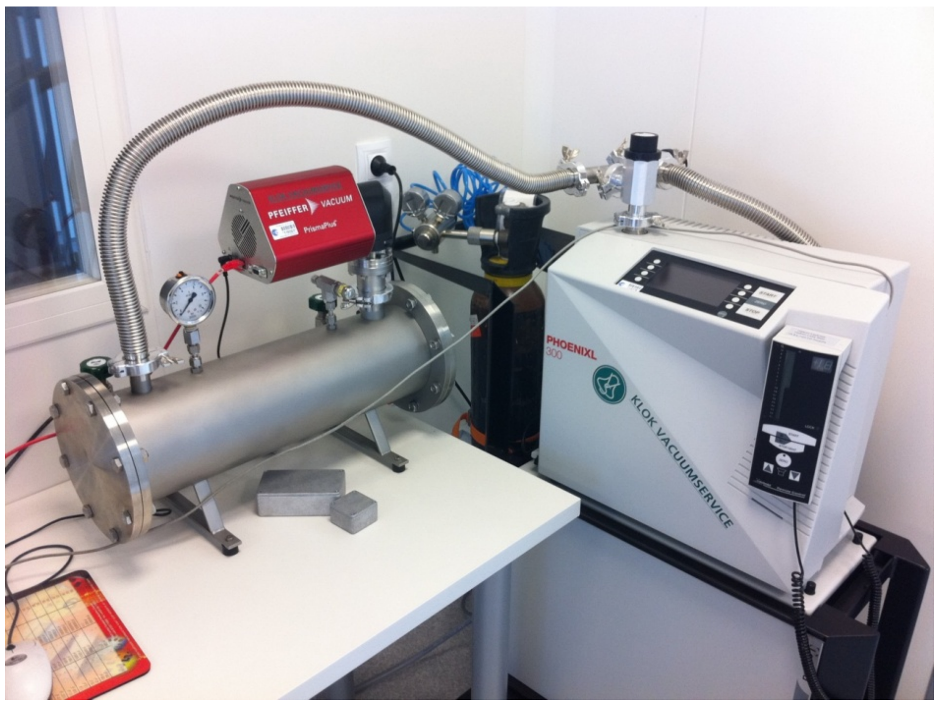

- Other activities related with the Space Materials laboratory:
- Atomic force microscopy (AFM)
- Masses spectrometry
- Electronic microscopy
- Nuclear magnetic resonance
- X-Ray diffraction for mono-crystals and poli-crystals materials
- X-Ray fluorescence

INDEX

- Monte-Carlo method developed for multipactor simulations:
- Electron tracking by solving relativistic Lorentz force:

$$\vec{F}_{\mathrm{L}} = q(\vec{E} + \vec{v} \times \vec{B}) = \frac{d\vec{p}}{dt}$$

$$\vec{p} = m_0 \gamma \vec{v} \qquad \frac{d\vec{p}}{dt} = m_0 \frac{d(\gamma \vec{v})}{dt}$$

$$\gamma = 1/\sqrt{(1-(v/c)^2)}$$

- Velocity-Verlet algorithm has been used for the numerical solution of the differential equations:
  - accurate
  - efficient
  - stable

- Effective electron model: each individual effective electron represents the charge (and the mass) of a set of electrons generated by itself.

E. Somersalo, P. Ylä-Oijala, and D. Proch, “Electron multipacting in RF structures”, Deutsches Elektronen-Synchrotron DESY, Hamburg (Germany), TESLA Rep. 94-14, Jul. 1994
P. Ylä-Oijala, “Analysis of electron multipacting in coaxial lines with traveling and mixed waves”, Deutsches Elektronen-Synchrotron DESY,Hamburg, Germany, TESLA Rep. 97-20, Nov. 1997

- Space charge effect (Coulombian repulsion): It has been considered in simple geometries, as parallel-plate guide and coaxial lines (planar or cylindrical sheet current with a uniform negative charge distribution)
- Nowadays we are using Darwin lagrangian for accounting space charge effect in arbitrarily-shaped components

- SEEY model:

$$\delta(W,\xi) = \begin{cases} 1 & \text{si} \quad \gamma < 1 \\ \delta_{max}(\xi)(\gamma e^{(1-\gamma)})^{0,25} & \text{si} \quad 1 < \gamma \leqslant 3{,}6 \\ \delta_{max}(\xi)\frac{1{,}125}{\gamma^{0,35}} & \text{si} \quad 3{,}6 < \gamma \end{cases}$$

$$\gamma = \frac{W - W_0}{W_{max}(\xi) - W_0}$$

$$\delta_{max}(\xi) = \delta_{max}(0) \cdot (1 + \frac{k_W \xi^2}{2\pi})$$

$$W_{max}(\xi) = W_{max}(0) \cdot (1 + \frac{k_\xi \xi^2}{2\pi})$$

- J.R.M. Vaughan "Secondary Emission Formulas", *IEEE Trans. Electron Devices, vol. 36, no. 9, p. 1963, Sep. 1989.*
- C.Vicente et al. "Multipactor breakdown prediction in rectangular waveguide based components", *IEEE MTT-S,* June 2005

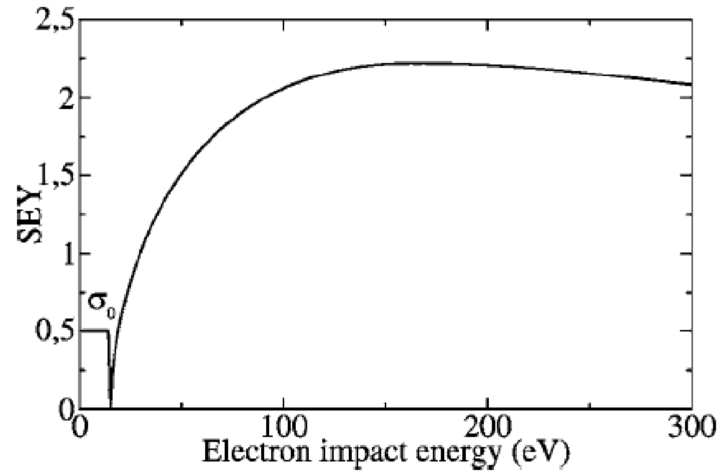

- <u>Multipactor effect in wedge-shaped waveguide:</u>
- Proposed in: E. Chojnacki, PRST-AB, vol. 3, no. 3, p. 032 001, 2000.
- Analyzed in: V. Semenov et al., IEEE Trans. Plasma Sci., vol. 36, no. 2, pp. 488–493, Apr. 2008.
- A resonant trapped electron trajectory is possible, but it is **unstable**: multipactor threshold is higher than in the corresponding rectangular guide.

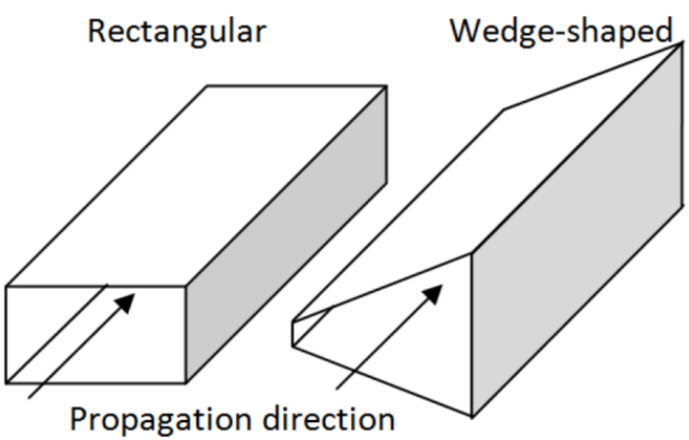

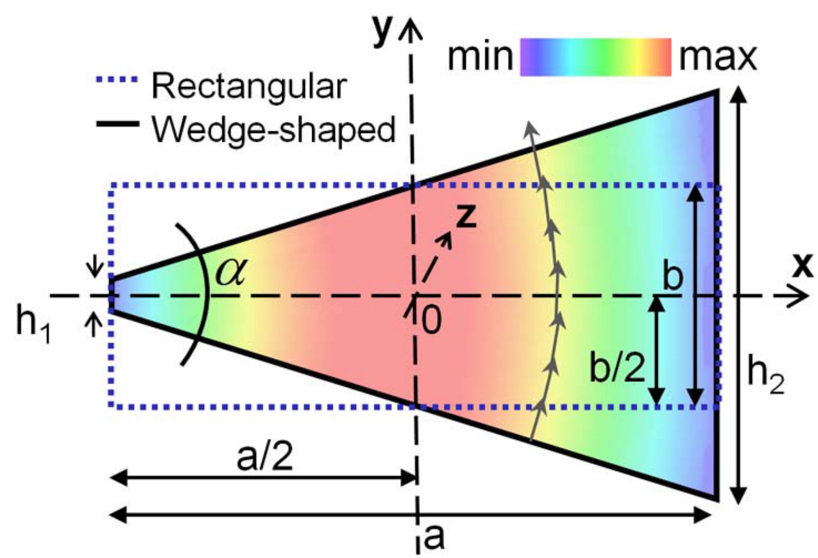

- Two prototypes have been designed, fabricated and tested:

RECTANGULAR

front view

perspective

WEDGE-SHAPED

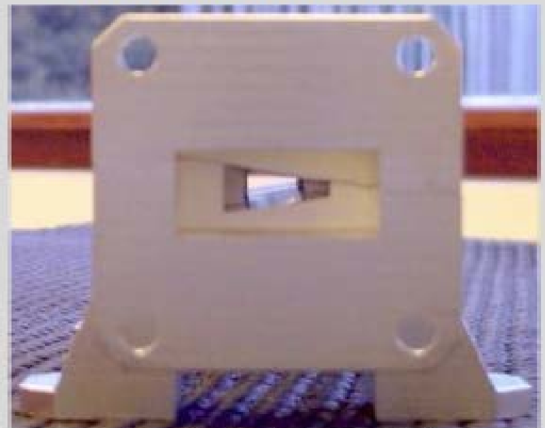

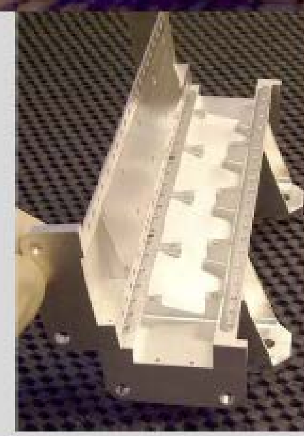

$\alpha = 19^\circ$ inclination

- Electrical response has been maintained in both band-pass filters. Simulations with FEST3D and HFSS:

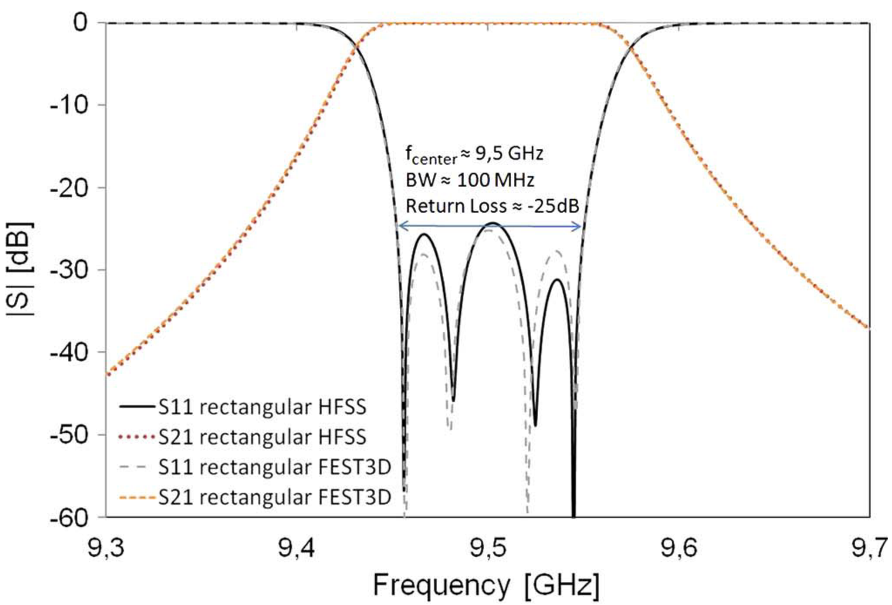

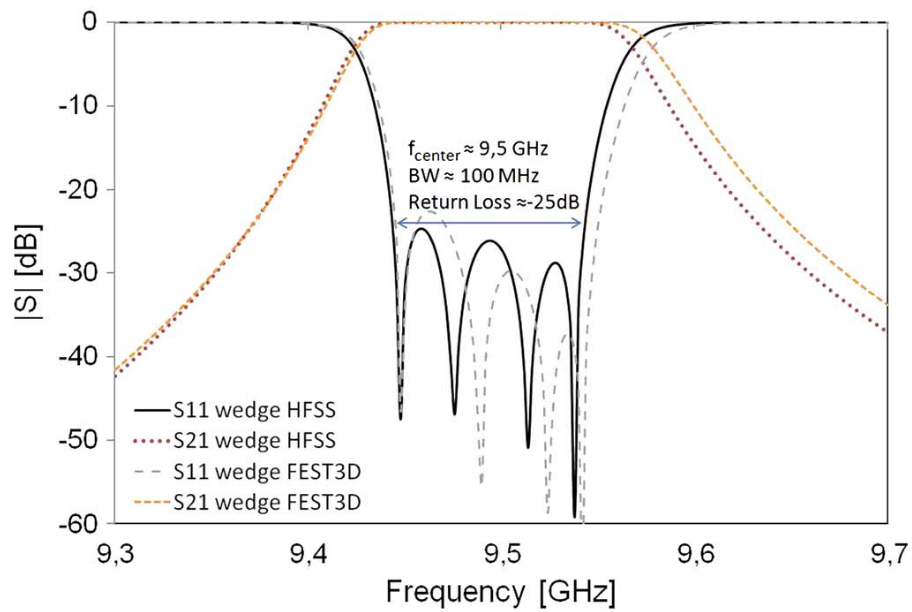

- Comparison between measurements and simulations:

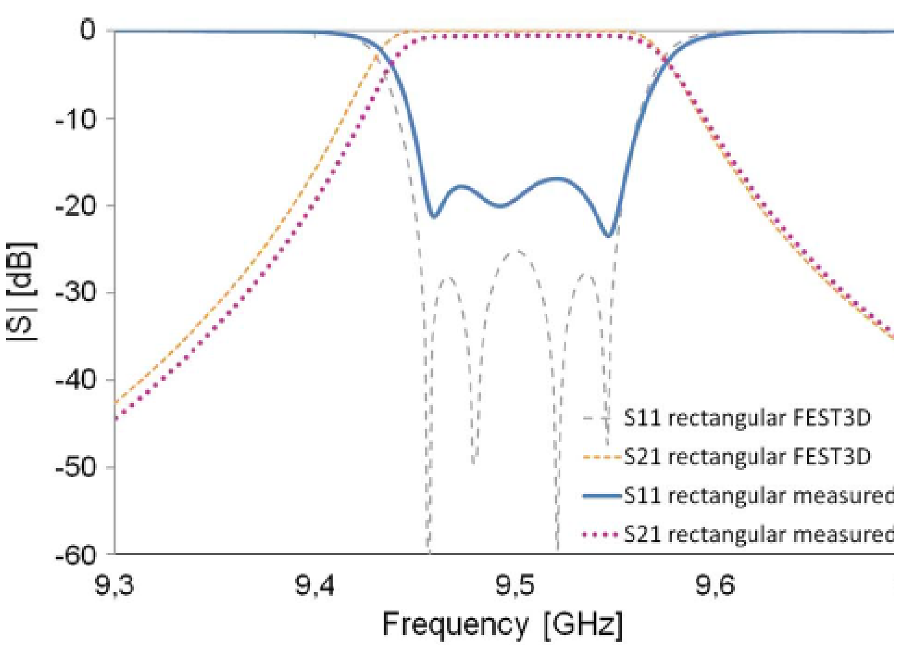

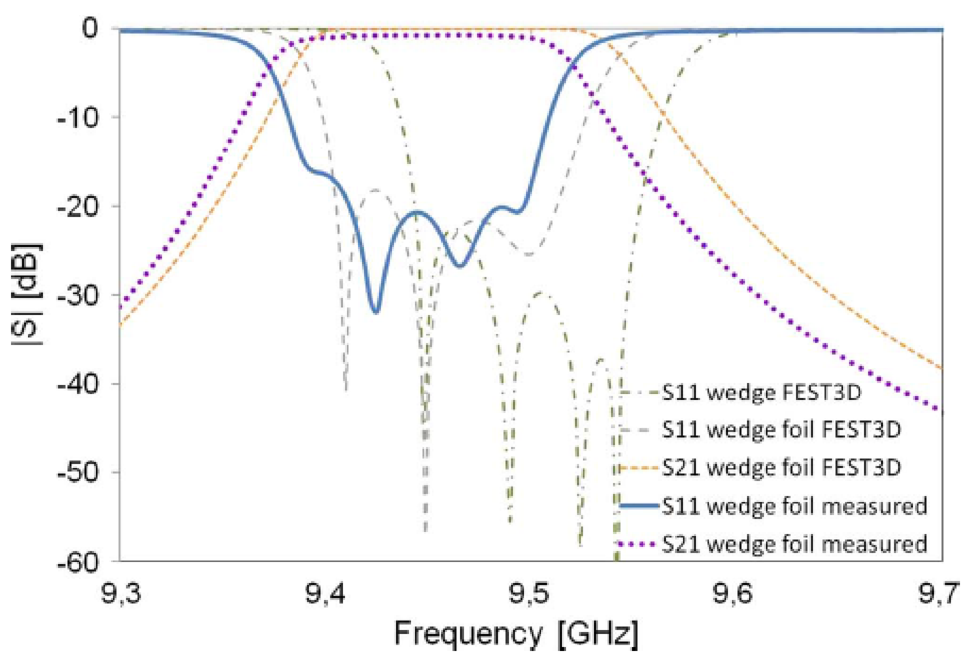

- Multipactor experimental test-bed:

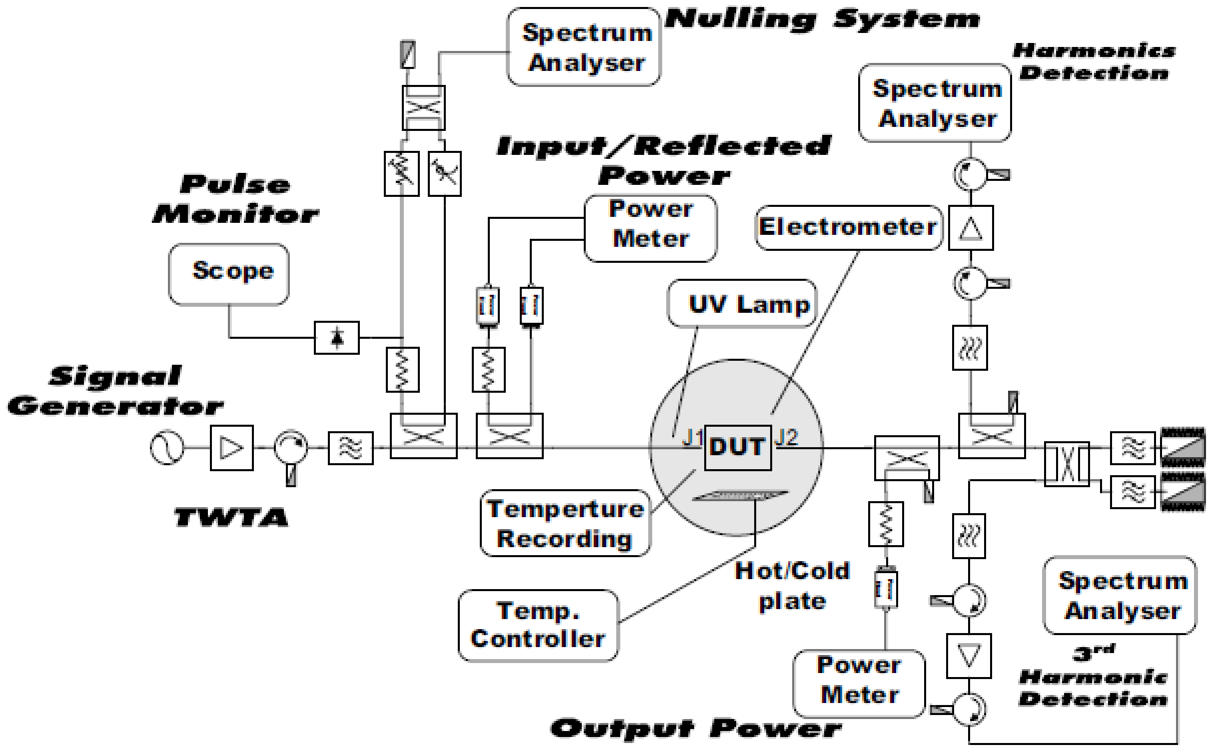

Figure 4. Test set-up used for the experiments performed at the ESA/ESTEC RF High-Power Laboratory.

R&D activities

- Diagnostic techniques of the experimental set-up:

- ➢ Nulling of the forward and the reflected signals (at the carrier frequency, f)
- ➢ Detection of the second (2*f) and/or third (3*f) harmonics of the carrier frequency
- ➢ Chamber pressure recording
- ➢ Detection of the emitted secondary electrons in the discharge by means of a Langmuir probe
- ➢ In next october we will start a project with Technical University of Madrid for the study of different Langmuir probes…
- ➢ Temperature recording

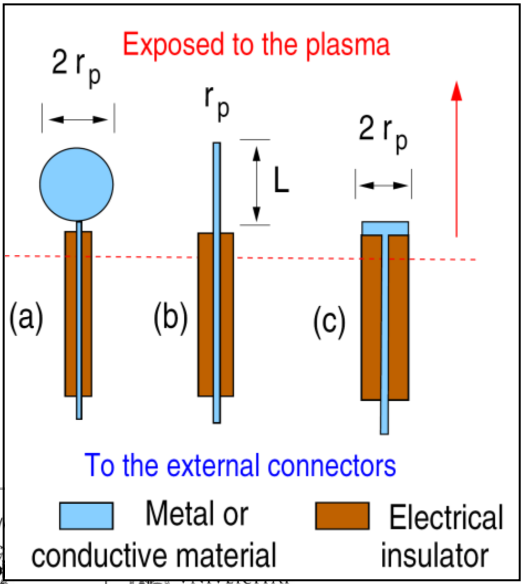

R&D activities

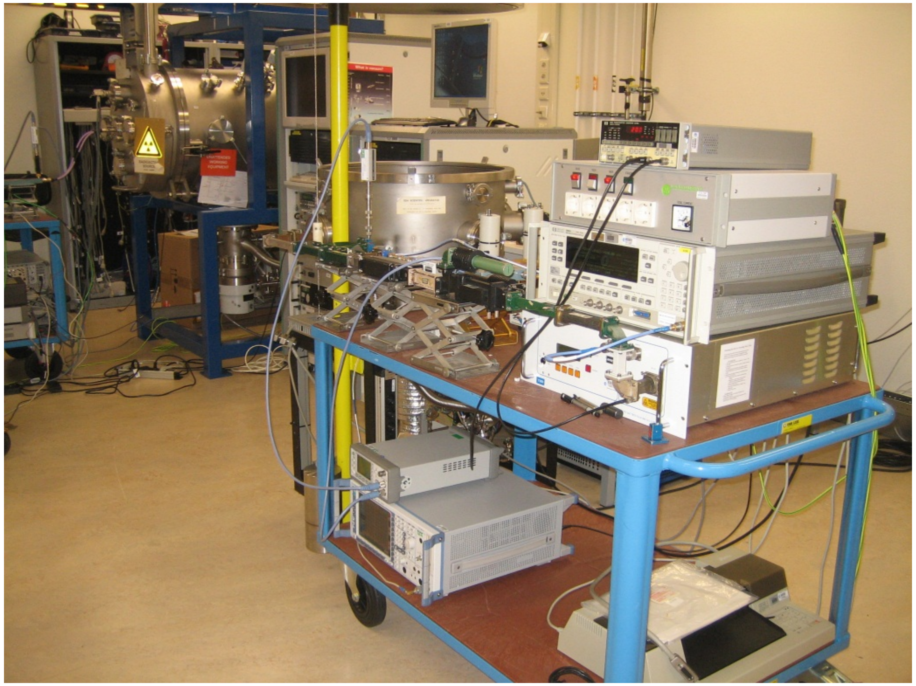

General view of the test-bed

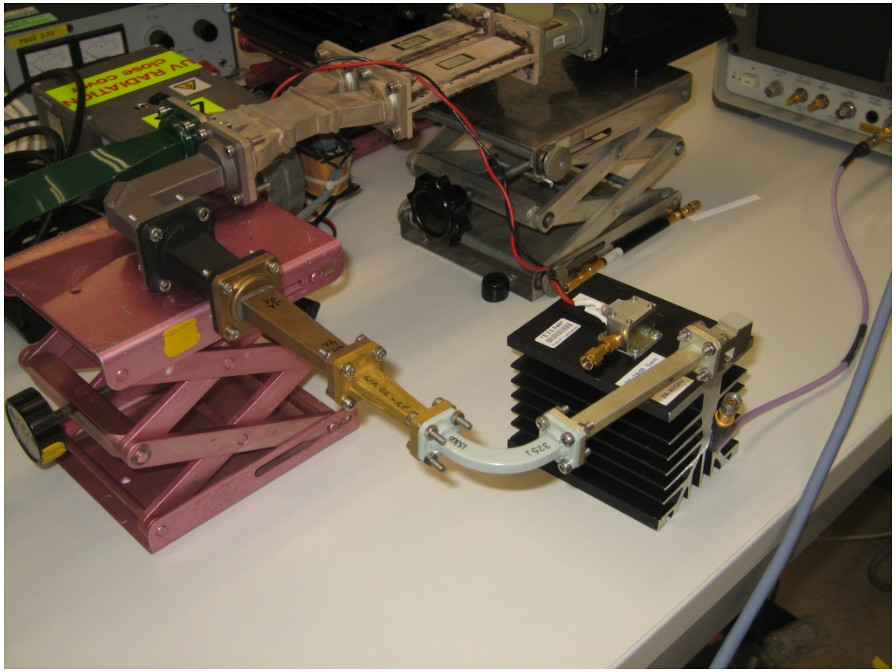

Third-harmonic detection waveguide taper

R&D activities

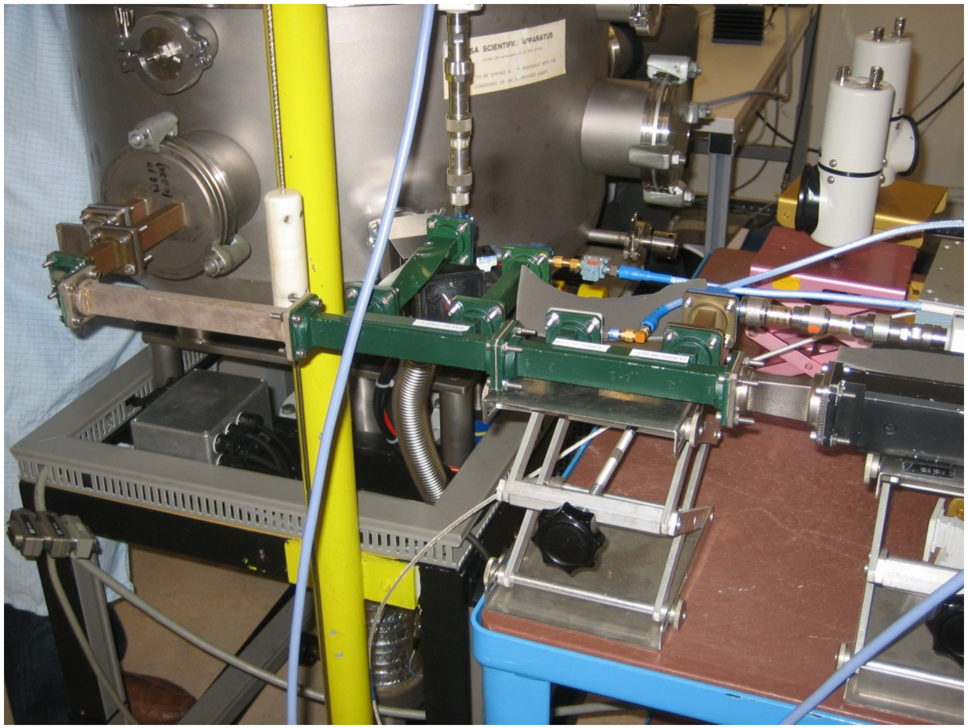

Detail of the waveguides entering to the vacuum chamber

Mr. David Raboso in action…

- Primary electron seeding used in the experimental set-up:

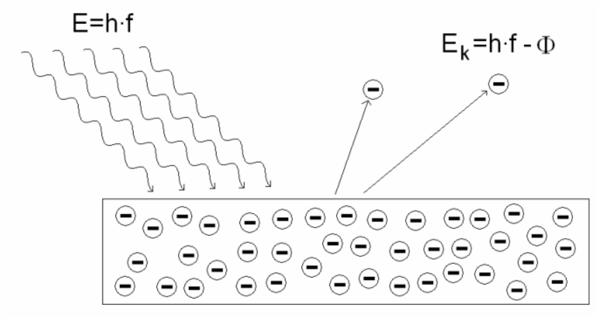

PHOTOELECTRIC EFFECT

^{90}Sr RADIOACTIVE SOURCE

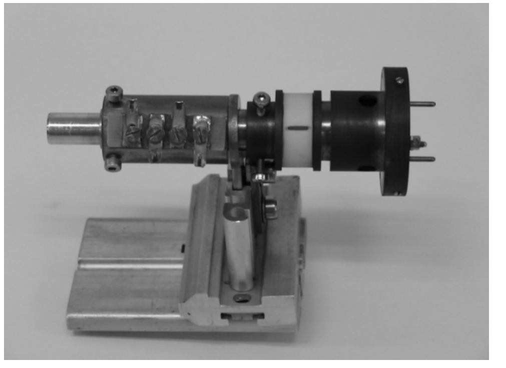

REGULATED ELECTRON GUN

- Theory has not been still developed.
- Need for theoretical simulations combined with experiments to study the influence of the seeding electron sources in the discharge onset.

- Comparison between experiment and multipactor simulations (performed with FEST3D):

Filter	Thresholds		
	ECSS MP Tool	$FEST^{3D}$	Measured
Rectangular @ 9.5 GHz	447 W	650 W	690 W
Wedge-shaped foil @ 9.45 GHz	558 W	1300 W	850 W

Potential benefit in the use of wedge-shaped filter: 0.91 dB

- Details can be found in:

J. Hueso et al., IEEE Trans. Electron Devices, vol. 57, no. 12, pp. 3508–3517, Dec. 2010.

J. Hueso et al., IEEE Trans. Electron Devices, vol. 58, no. 9, pp. 3205–3212, Sept. 2011.

R&D activities

- <u>Multipactor effect in coaxial lines considering an axial DC magnetic field:</u>
- Partial mitigation of the multipactor effect: RF breakdown power threshold can be raised up !!
- A big solenoid has been designed, manufactured and calibrated:

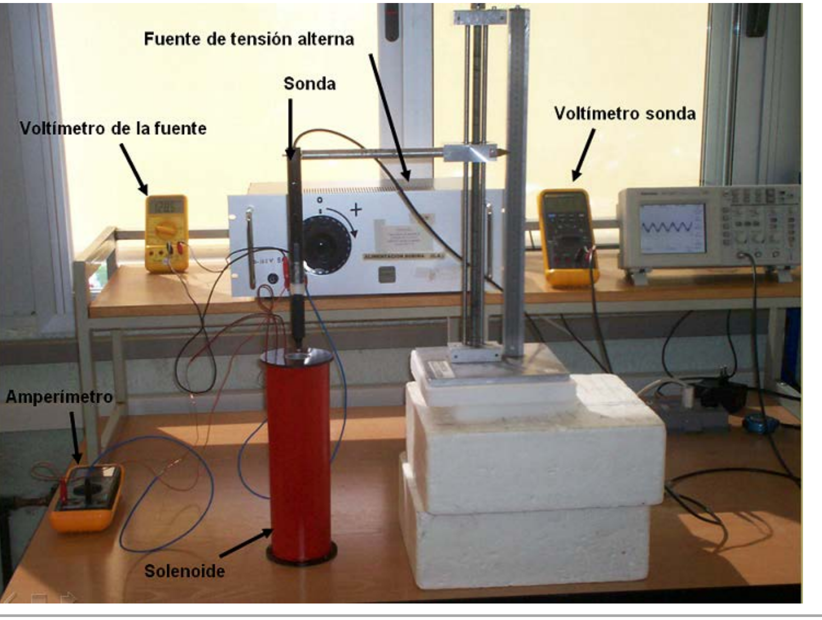

- Calibration curve of the solenoid:

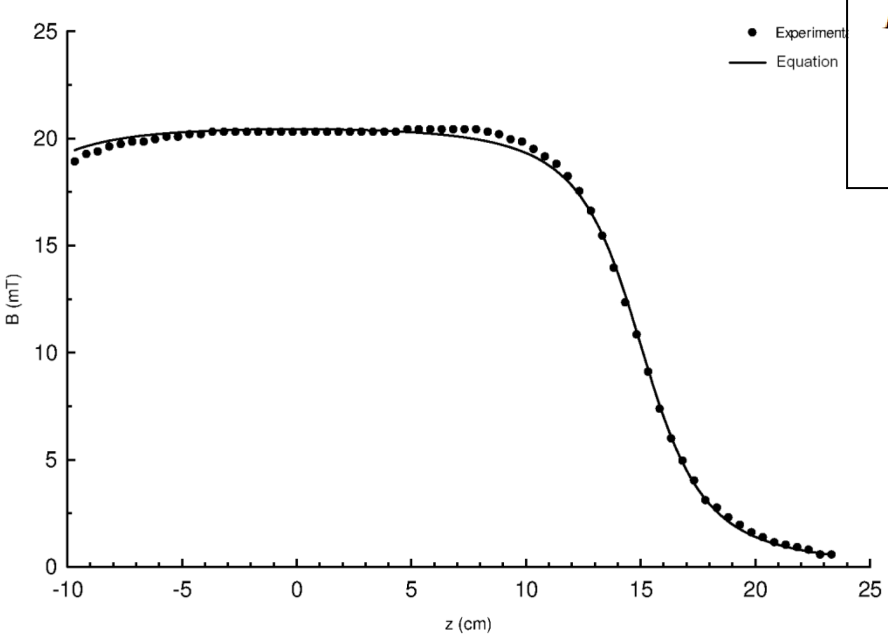

$$B_z(0,0,z)=\frac{\mu_0}{2}\frac{N\cdot I}{h}\left\{\frac{z+\frac{h}{2}}{\left[a^2+\left(z+\frac{h}{2}\right)^2\right]^{\frac{1}{2}}}-\frac{z-\frac{h}{2}}{\left[a^2+\left(z-\frac{h}{2}\right)^2\right]^{\frac{1}{2}}}\right\}$$

I: DC current feeding the solenoid
z: axial coordinate in the axis
a: mean radius = 2.93 cm
H: length = 30 cm
N: number of turns = 9248
(Electrical resistance = 71.8 Ω)

In the center of the solenoid a DC magnetic field of 3.8 mT for I=100 mA is detected.

- Coaxial sample:

a: inner radius = 1.515 mm
b: outer radius = 3.490 mm
d: gap = b – a = 1.975 mm
total length = 90.4 mm

- The sample is inserted in the middle of the coil:

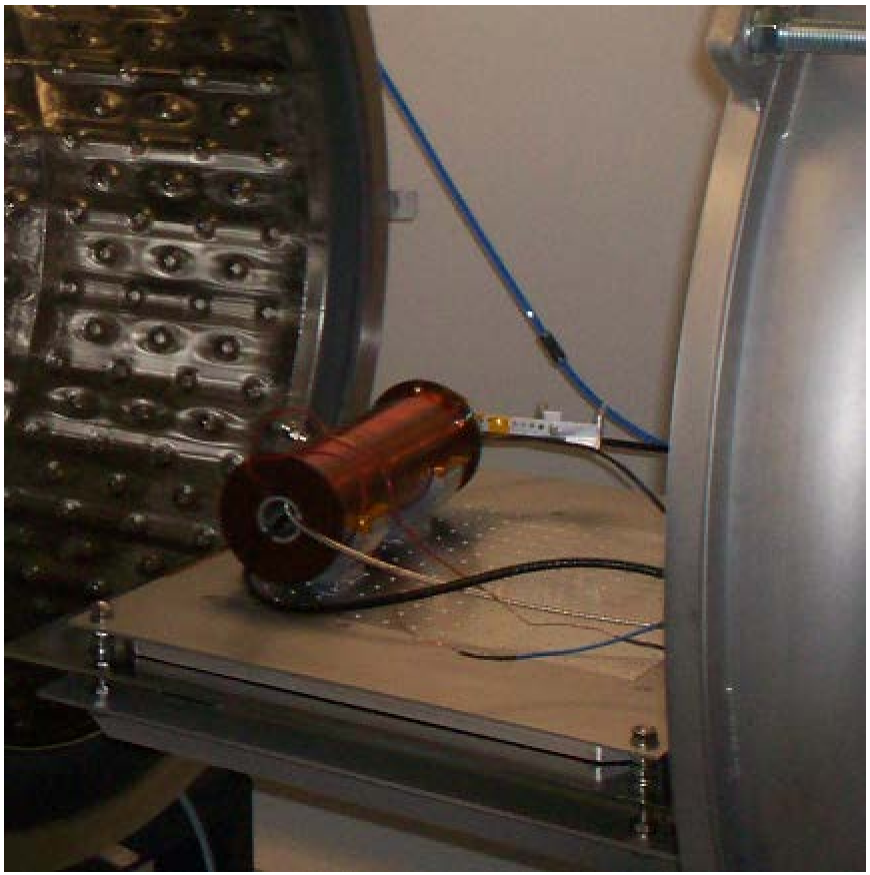

Multipactor diagnostic has been performed using the previous experimental test-bed: the RF breakdown power threshold has been measured as a function of the axial magnetic field (modifying the I DC driven current)…

- Comparison between experiment and simulations (FEST3D):

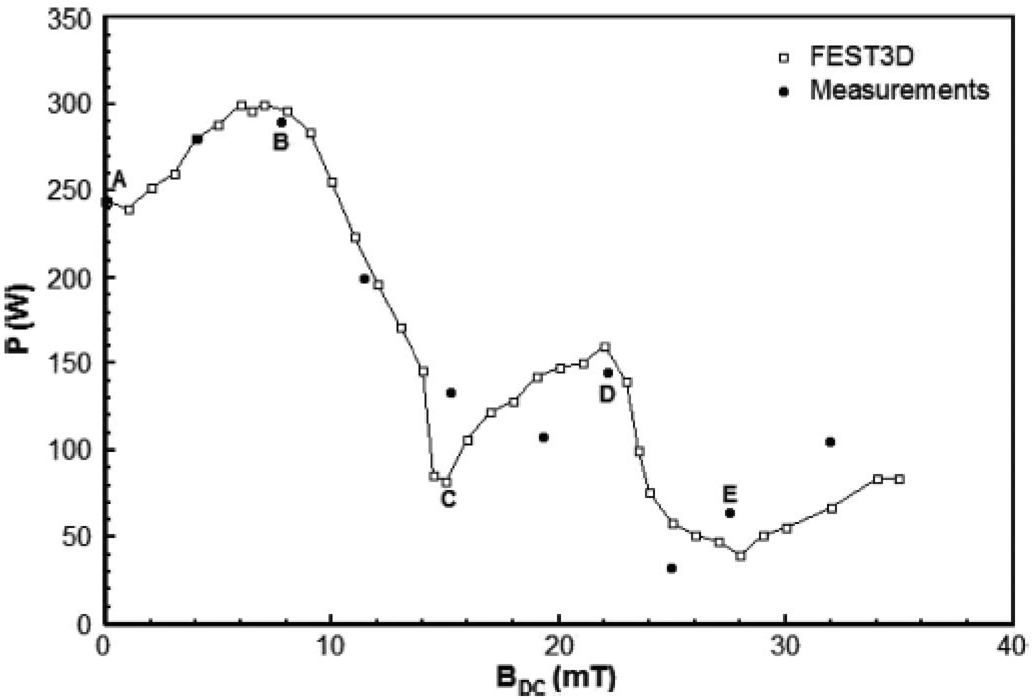

Fig. 2. Multipactor RF input power threshold as a function of the dc magnetic field strength. Experimental and theoretical results are shown. Experimental errors associated with both magnitudes have been estimated in ±2 W and ±1 mT, respectively.

TABLE I
SUMMARY OF THE RESULTS SHOWED IN FIG. 2

Point	B_{DC}(mT)	P(W)	f_c(MHz)	$r_L(\mu m)$	SEY_i	SEY_o
A	0	245	0	∞	2.0	1.1
B	8	290	216	875	2.9	2.9
C	15	86	420	449	1.2	0.5
D	22	145	620	305	0.4	1.1
E	27	65	770	245	2.2	0.9

R&D activities

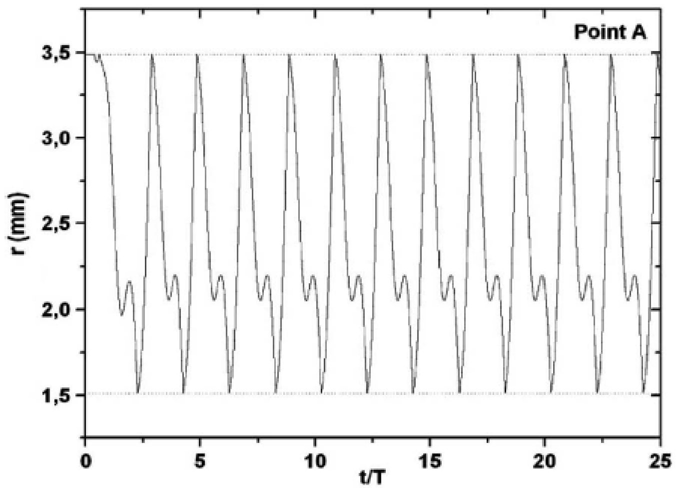

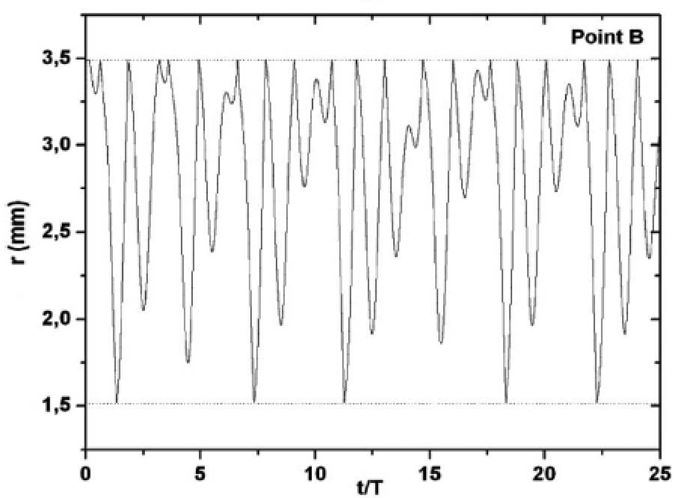

Point A:

We find a double-surface multipactor mode of order 3.

Point B:

We have observed a mixing between double- and single-surface multipactor regimes: the DC magnetic field tends to bend the electron orbits around the magnetic field flux lines. Threshold is higher than for the point A !

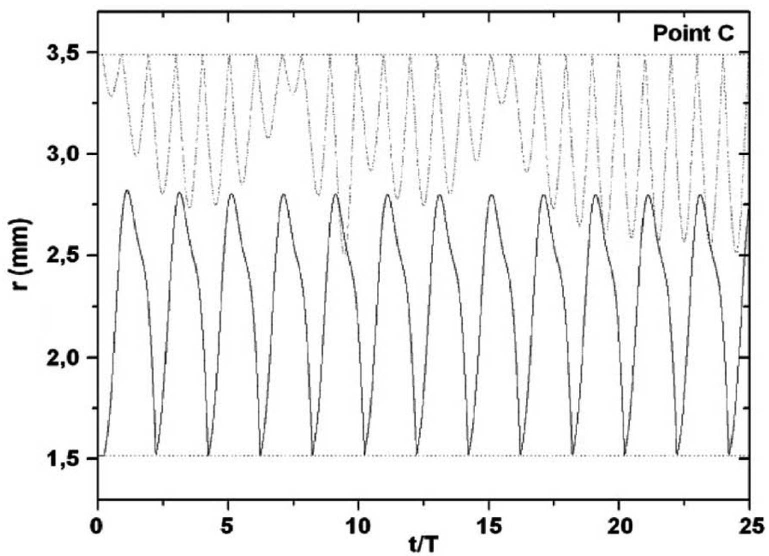

Point C:

Electrons launched from the inner conductor: the dc magnetic field is strong enough to avoid electrons reaching the opposite conductor so that there are only single-surface orbits. Discharge is generated only on the inner wall.

Electrons launched from the outer conductor: they impact with low energy so they do no generate secondaries.

R&D activities

Point D:

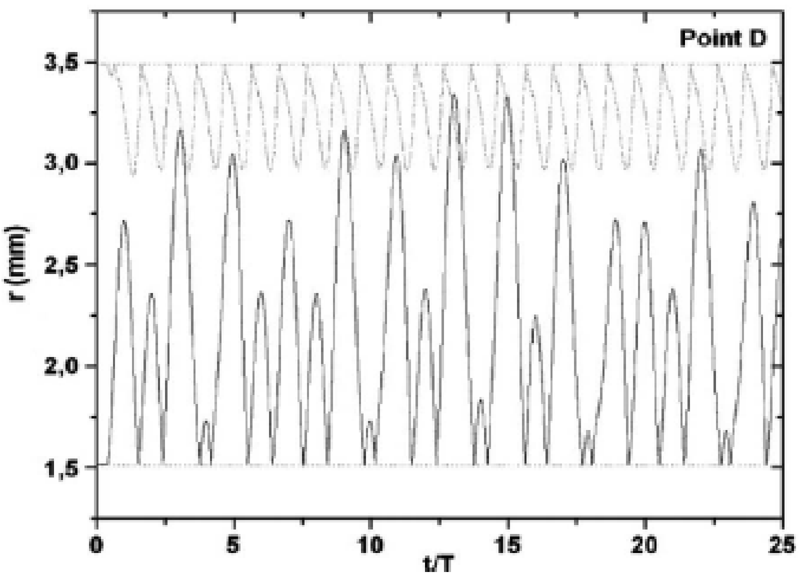

In the range from point C to point D: multipactor cannot occur on the inner wall because of a lack of resonance.

In the outer conductor:
A stable single-surface discharge of order 2 can be generated on the outer metal. Significant local increase in the threshold of point D is explained in terms of the variation with the radial coordinate of the applied RF electric field.

- Details can be found in:

D. González-Iglesias, A. M. Pérez, S. Anza, J. Vague, B. Gimeno, V. E. Boria, D. Raboso, C. Vicente, J. Gil, F. Caspers, L. Conde, IEEE Electron Devices Letters, vol. 33, no. 5, pp. 727–729, May 2012.

- Multipactor effect with dielectrics:

- Analysis of a dielectric-loaded parallel-plate waveguide:

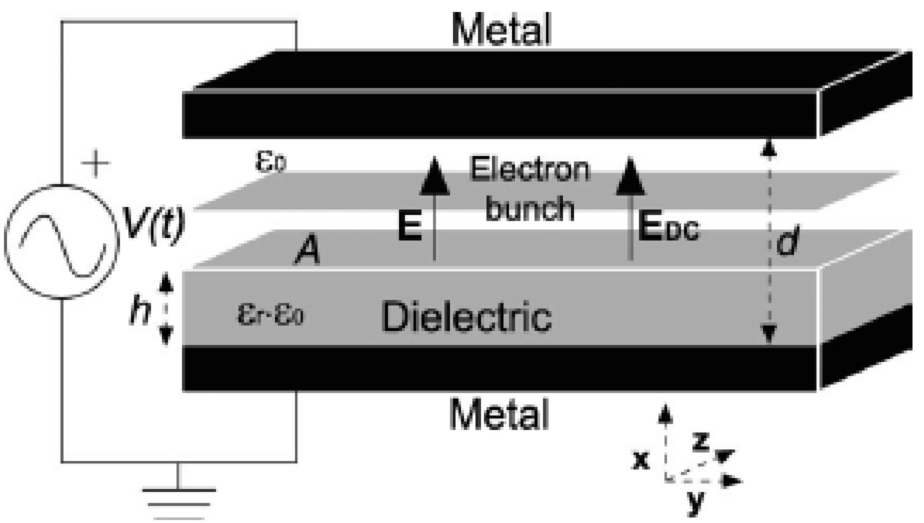

Space charge effect is considered by means of a dynamic planar sheet uniformly charged containing the electrons generated during the discharge (in both dielectric and metallic surfaces).

The effect of the time-varying static electric field generated by the emission (positive) or absortion (negative) of electrons colliding against dielectric surface has been accounted.

Partial mitigation of the discharge due to the static electric field generated on the dielectric surface: two regimes have been found...

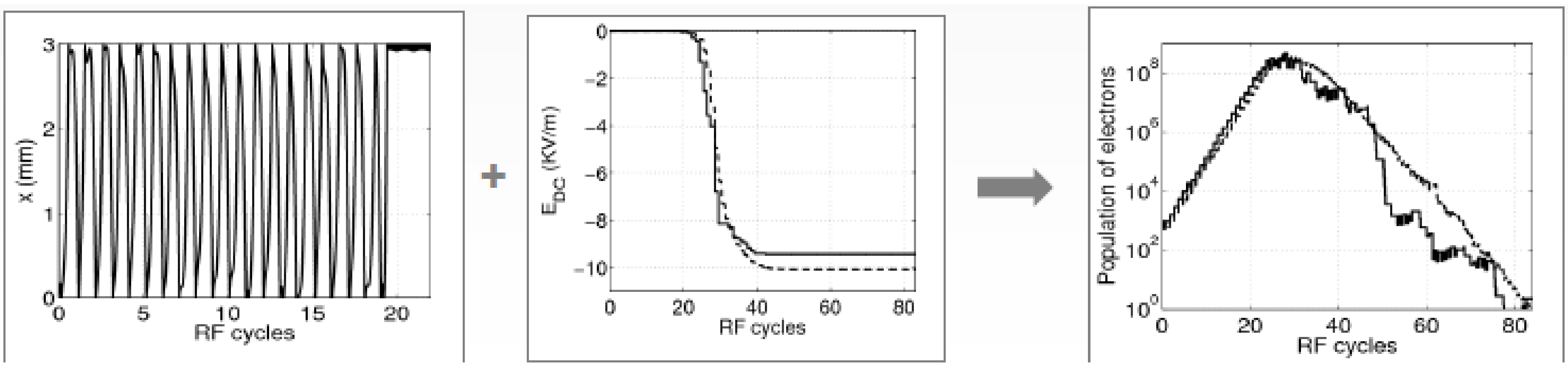

Electrons are absorbed on the dielectric surface: static electric field is negative and electrons are repelled, destroying the resonance; finally discharge is turned off by itself

G. Torregrosa, Á. Coves, C. P. Vicente, A.M. Pérez, B. Gimeno, V. E. Boria, IEEE Electron Devices Letters, vol. 27, no. 7, pp. 619–621, July 2006.

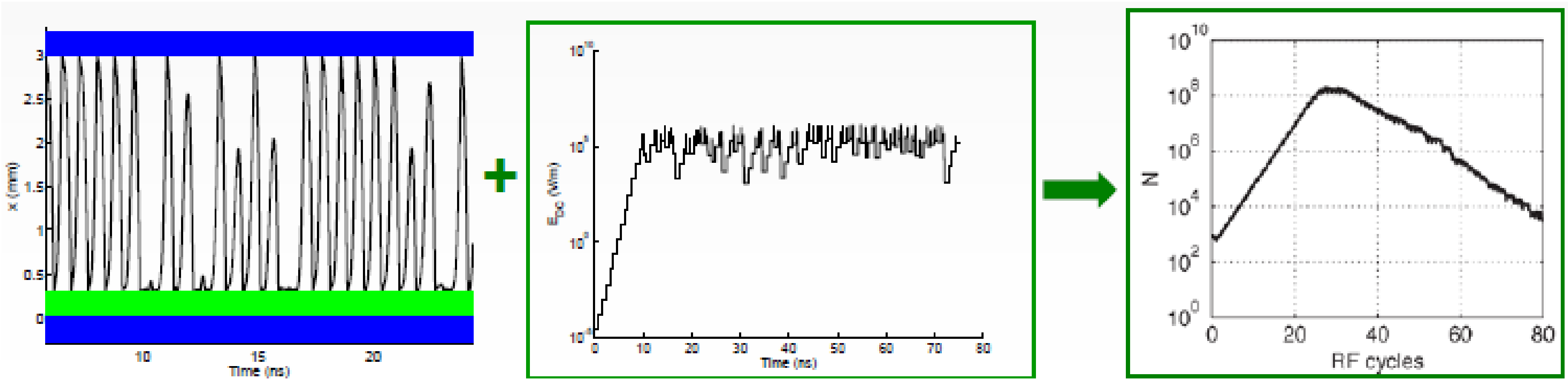

Electrons are emitted from the dielectric surface: static electric field is positive and electrons are attracted, destroying the resonance; finally discharge is turned off by itself

Á. Coves, G. Torregrosa-Penalva, C. Vicente, B. Gimeno, V. E. Boria, IEEE Trans. Electron Devices, vol. 55, no. 9, pp. 2505-2511, Sept. 2008

Computation of multipactor susceptibility charts as a function of geometrical and electrical parameters:

G. Torregrosa-Penalva, Á. Coves, B. Gimeno, I. Montero, C. Vicente, V. E. Boria, IEEE Trans. Electron Devices, vol. 57, no. 5, pp. 1160-1166, May 2010

- Analysis of a dielectric-loaded rectangular cavity for THALES ALENIA SPACE ESPAÑA with the software SPARK3D (2.333 GHz)

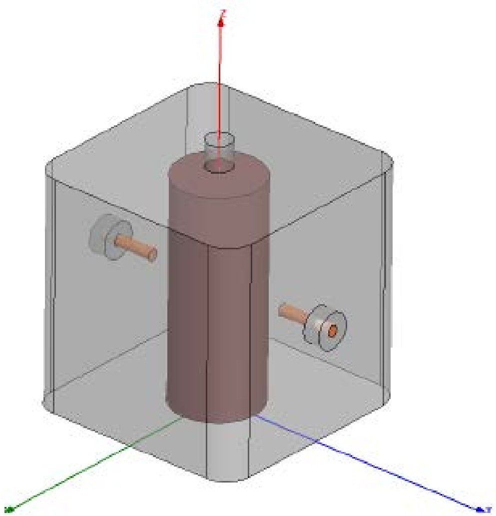

RF input power threshold

Simulation: 443 mW
Experiment: 430 mW

- Multipactor effect in circular waveguides:

- Monte-Carlo algorithm has been transformed in order to consider the degenerate fundamental TE_{11} circular mode considering orthogonal polarizations ($TE_{11}^{(c)}$ and $TE_{11}^{(s)}$):

$$E_r = -A_{11}\frac{1}{\varepsilon r}J_1(\beta_r r)(\sin(\varphi)\cos(\omega t) + AR\cos(\varphi)\cos(\omega t+\phi))$$

$$E_\varphi = A_{11}\frac{\beta_r}{\varepsilon}J_1'(\beta_r r)(\cos(\varphi)\cos(\omega t) + AR\sin(\varphi)\cos(\omega t+\phi))$$

$$H_z = -A_{11}\frac{\beta_r^2}{\omega\mu\varepsilon}J_1(\beta_r r)(\cos(\varphi)\sin(\omega t) + AR\sin(\varphi)\sin(\omega t+\phi))$$

$$\boxed{V_{eq} = 2\int_0^{d/2} E_r(r,\varphi=\pi/2,\omega t=0)dr}$$

2D non-relativistic electron motion differential equations consider both centripetal and Coriolis accelerations:

$$\ddot{r} = \frac{-e}{m}\left[E_r(r,\varphi,t) + r\dot{\varphi}B_z(r,\varphi,t)\right] + r\dot{\varphi}^2$$

$$r\ddot{\varphi} = \frac{-e}{m}\left[E_\varphi(r,\varphi,t) - \dot{r}B_z(r,\varphi,t)\right] - 2\dot{r}\dot{\varphi}$$

- Comparison with a parallel-plate guide (with only vertical polarization):

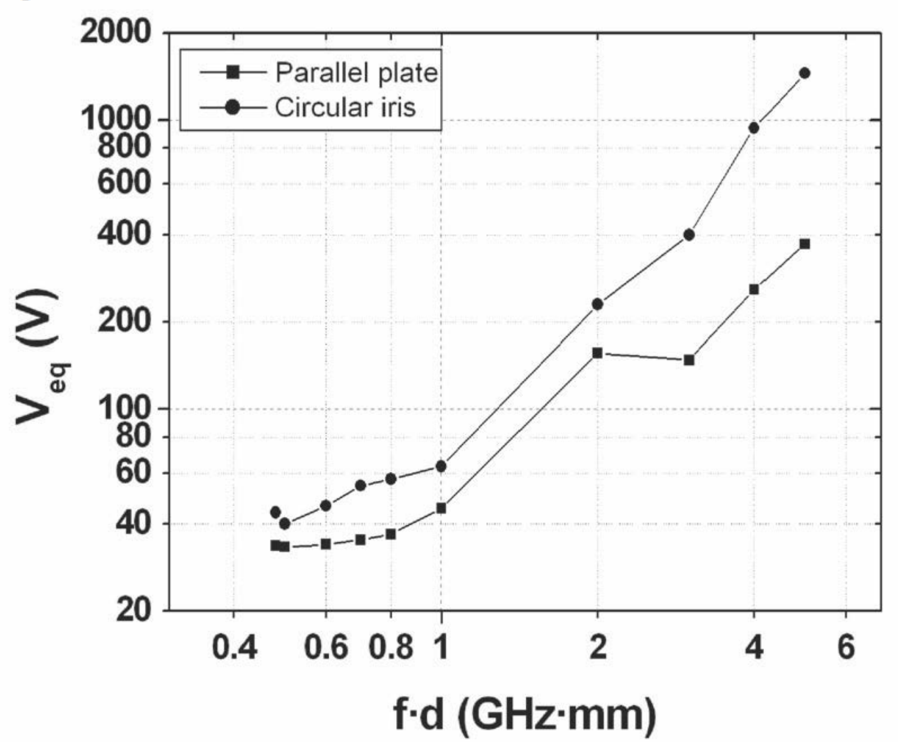

- Study of the multipactor stability (with only vertical polarization) for a case of f*d = 1 GHzmm:

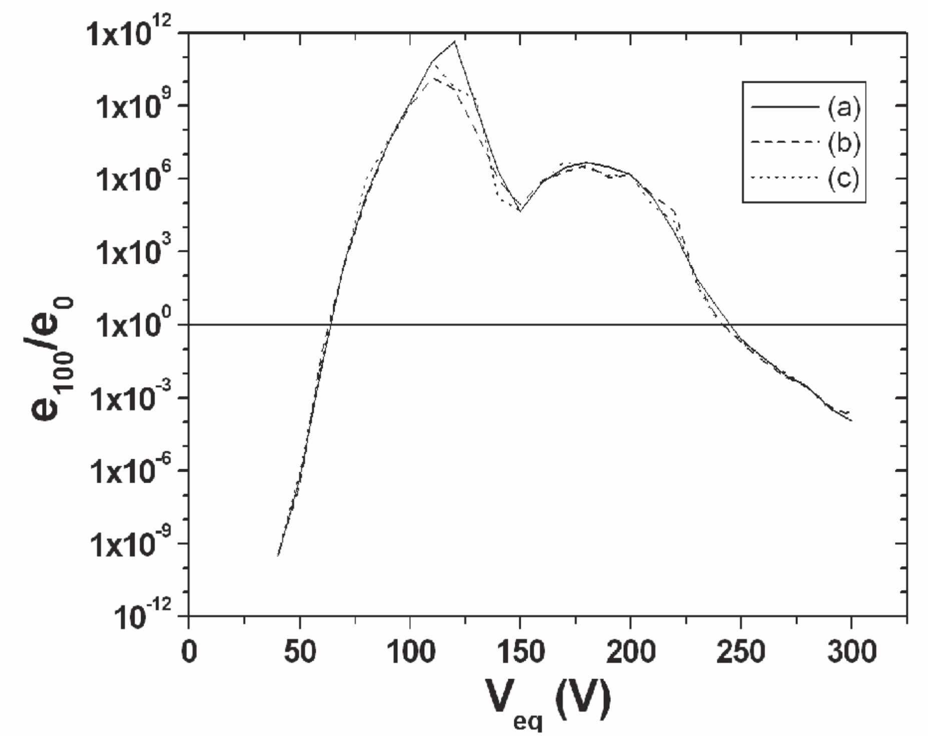

(a) d = 0.5mm and f = 2GHz

(b) *d = 1mm and f = 1 GHz*

(c) d = 2mm and f = 0.5GHz

A.M. Pérez, V.E. Boria, B. Gimeno, S. Anza, C. Vicente, J.Gil, Journal Electromag. Waves and Applications, vol. 23, pp. 1575-1583, 2009

- Resonant effective electron orbits for the first 30 impacts: double-surface multipactor events are observed for different values of AR

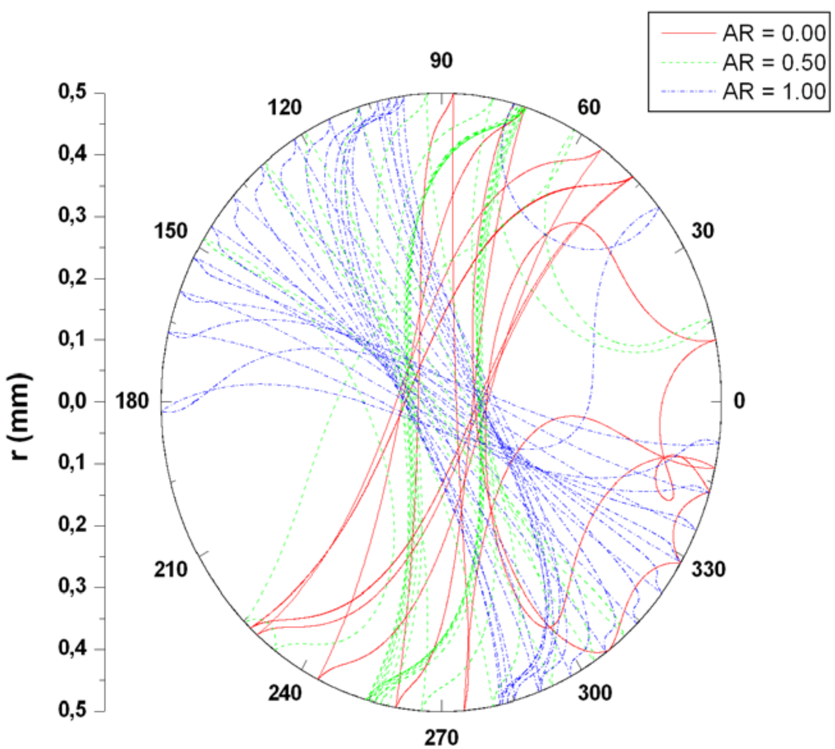

d =1 mm and f = 1 GHz
(f*d = 1 GHzmm)

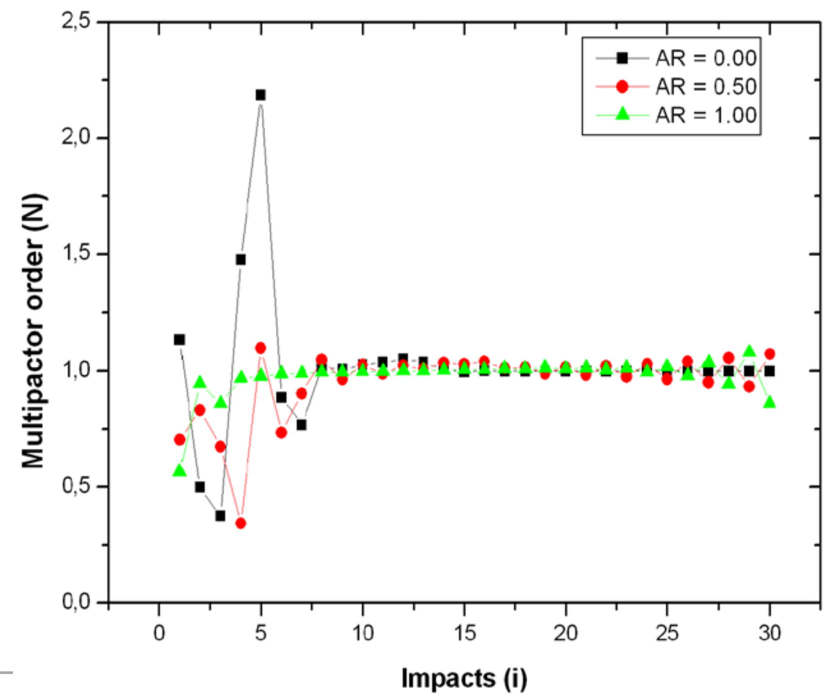

- <u>Multipactor effect in elliptical waveguides</u>:

- Monte-Carlo algorithm has been transformed in order to consider the fundamental $TE_{11}^{(c)}$ elliptical mode

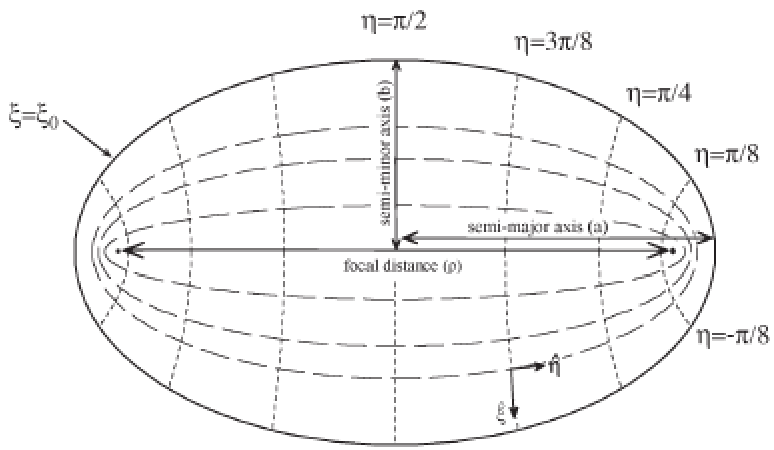

Fig. 1. Planar elliptical coordinate system. The semimajor axis length is a, the semiminor axis length is b, and the focal distance is ρ.

$$\ddot{\xi} = -\frac{e}{\rho\, m\sqrt{U}}\left[E_\xi(\xi,\eta,t) + \rho\dot{\eta}\sqrt{U}B_z(\xi,\eta,t)\right] - \left[(\dot{\xi}^2 - \dot{\eta}^2)\sinh(2\xi)/2 + \dot{\xi}\dot{\eta}\,\sin(2\eta)\right]/U$$

$$\ddot{\eta} = -\frac{e}{\rho\, m\sqrt{U}}\left[E_\eta(\xi,\eta,t) + \rho\dot{\xi}\sqrt{U}B_z(\xi,\eta,t)\right] - \left[(\dot{\eta}^2 - \dot{\xi}^2)\sin(2\eta)/2 + \dot{\xi}\dot{\eta}\,\sinh(2\xi)\right]/U$$

$$U = \sinh^2(\xi) + \sin^2(\eta).$$

2D non-relativistic electron motion differential equations have been numerically solved

- A double-surface first-order multipactor discharge is observed:

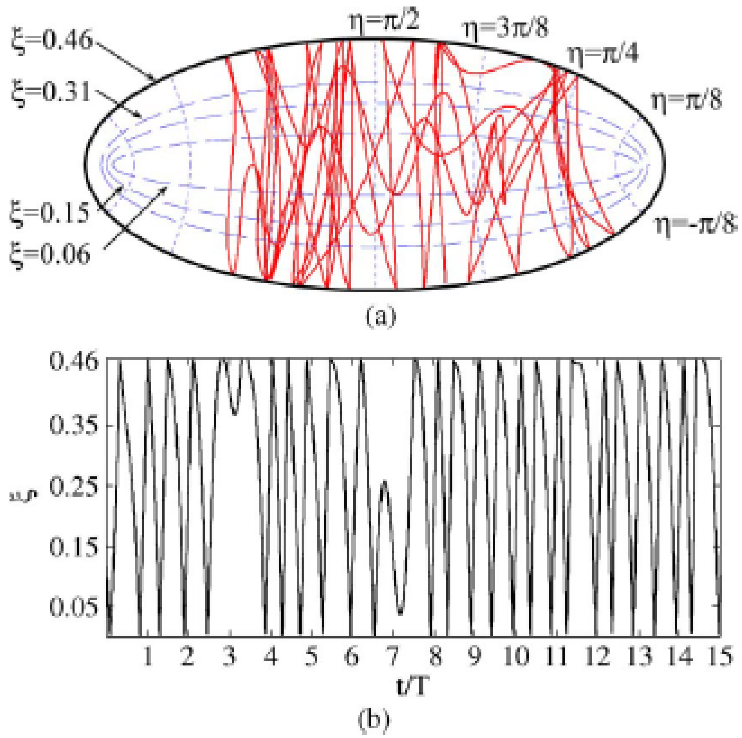

Fig. 2. (a) Electron motion in an elliptical waveguide. (b) Radius of an effective electron versus normalized time.

- Stability of the multipactor mode has been studied:

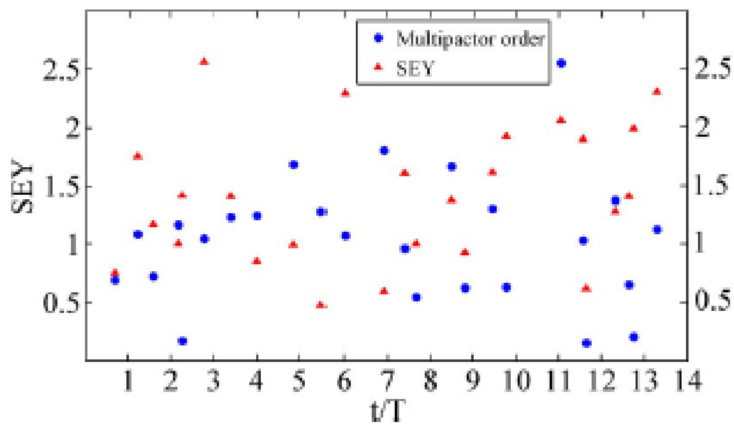

Fig. 3. SEY coefficients and multipactor orders as a function of the normalized time.

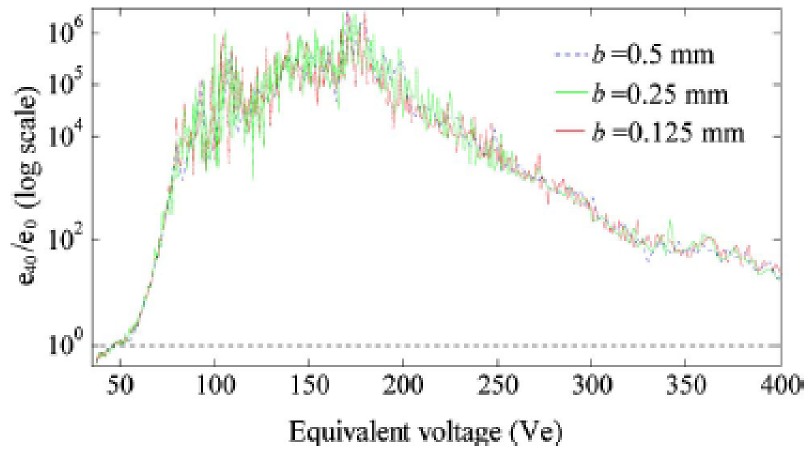

Fig. 4. Enhanced counter function as a function of the equivalent voltage for three different values of the semiminor axis length when $f \times d = 1$.

- Voltage threshold has been computed for an iris; elliptical eccentricity has been changed::

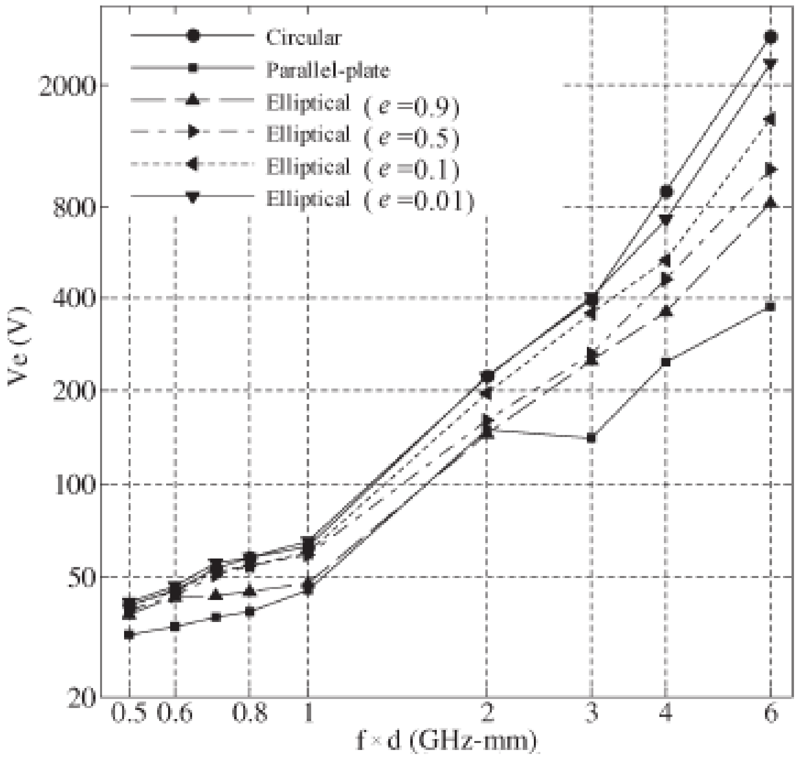

Fig. 5. Multipactor breakdown thresholds in an elliptical waveguide for four different values of eccentricity compared with multipactor breakdown thresholds in parallel-plate and circular waveguides ($f = 1$ GHz).

A. Frotanpour, G. Dadashzadeh, M. Shahabadi, B. Gimeno, IEEE Trans. Electron Devices, vol. 58, no. 3, pp. 876-881, March 2011

- Multipactor effect in complex structures:

- E-plane transformer implemented in rectangular waveguide

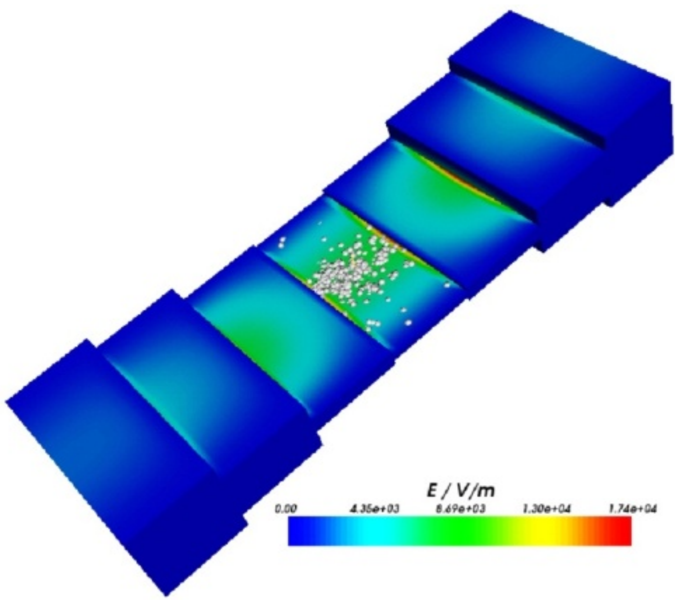

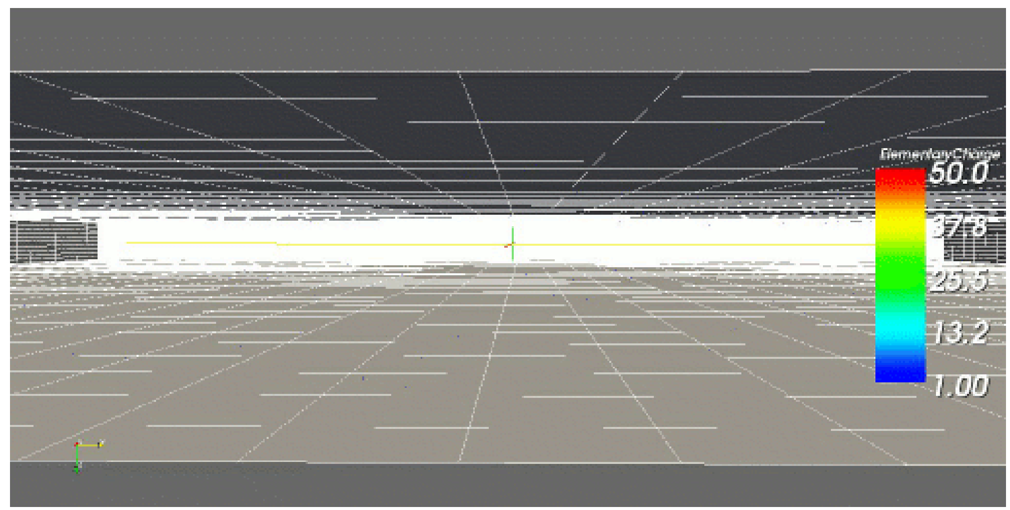

MULTIPACTOR SIMULATION IN THE CENTRAL IRIS

R&D activities

- Multipactor effect in a rectangular iris of a high-power dual-mode band-pass filter implemented in rectangular waveguide:

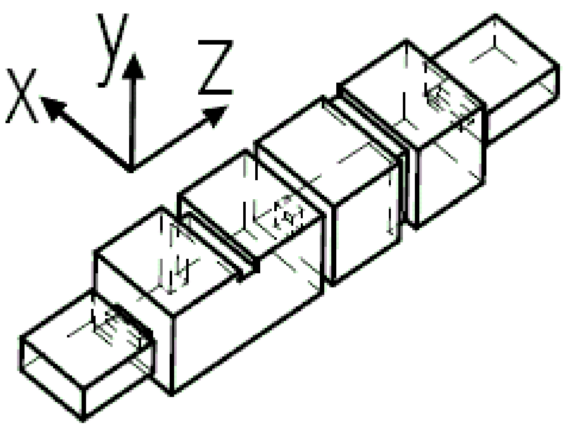

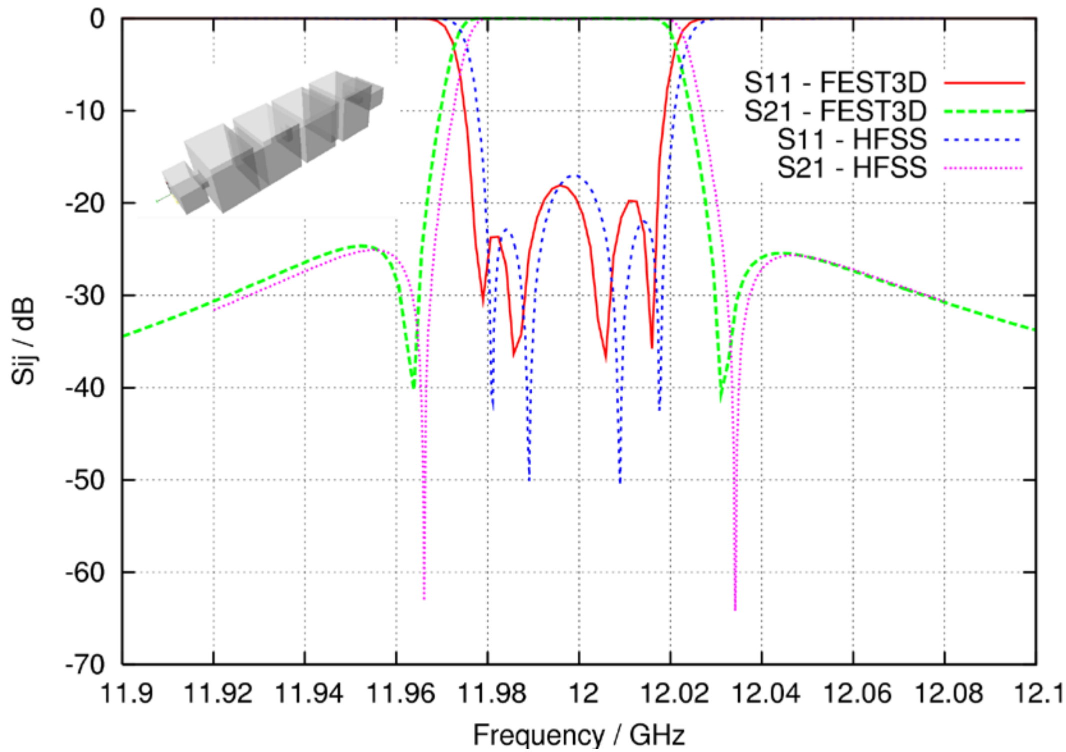

Multipaction simulation: electrons escape from the iris due to the fringing fields (axial drift); as a consequence, the RF breakdown power threshold is lower than in an “infinite” guide

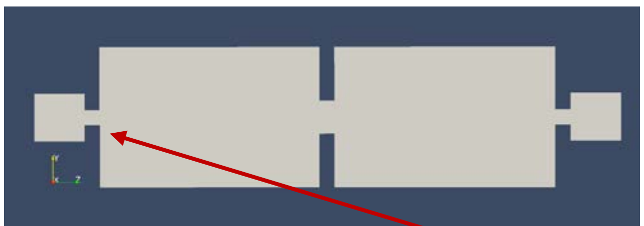

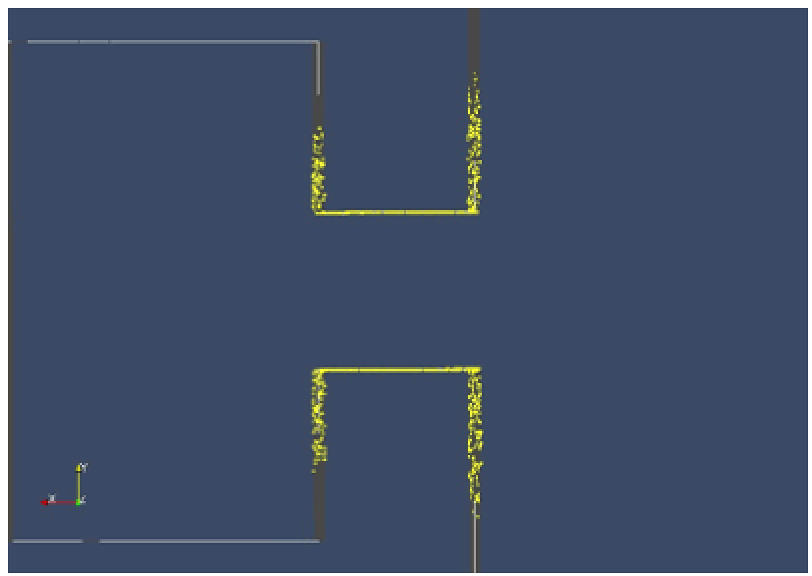

- <u>Electromagnetic radiation within waveguides</u>:
- A charged particle is moving within an arbitrarily cross-shaped waveguide:

$$\boxed{\vec{J}(x,y,z,t) \sim -e\,\vec{v}(x,y,z,t)} \longrightarrow \boxed{\vec{J}(x,y,z,\omega) \sim -e\,\vec{v}(x,y,z,\omega)}$$

FOURIER TRANSFORMATION

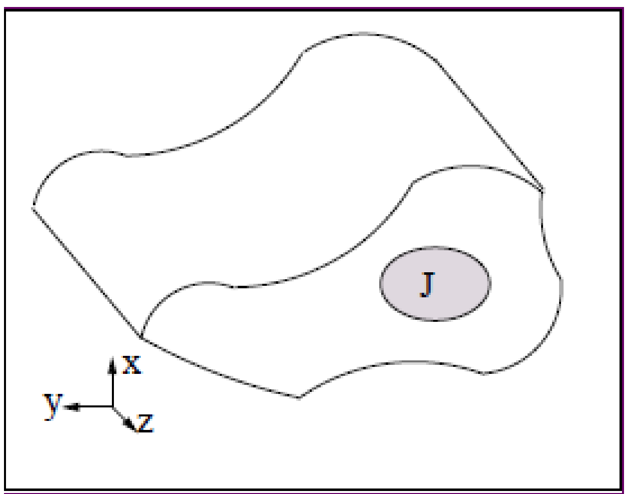

$$\nabla \cdot \vec{E} = \rho/\varepsilon_0$$
$$\nabla \cdot \vec{H} = 0$$
$$\nabla \times \vec{E} = -j\omega\mu_0\vec{H}$$
$$\nabla \times \vec{H} = \vec{J} + j\omega\varepsilon_0\vec{E}$$

Electromagnetic fields and singular current density in frequency domain are expressed in transverse and axial components:

$$\vec{E}(x,y,z) = \vec{E}_t(x,y,z) + E_z(x,y,z)\hat{z}$$
$$\vec{H}(x,y,z) = \vec{H}_t(x,y,z) + H_z(x,y,z)\hat{z}$$
$$\vec{J}(x,y,z) = \vec{J}_t(x,y,z) + J_z(x,y,z)\hat{z}$$

$$\nabla = \nabla_z + \hat{z}\frac{\partial}{\partial z}$$

$$\frac{\partial \vec{E}_t}{\partial z} = -j\omega\mu_o \vec{H}_t \times \hat{z} + \frac{1}{j\omega\varepsilon_o}\nabla_t\left(\nabla_t \cdot \left(\vec{H}_t \times \hat{z}\right) - J_z\right)$$
$$\frac{\partial \vec{H}_t}{\partial z} = -j\omega\varepsilon_o \hat{z} \times \vec{E}_t + \frac{1}{j\omega\mu_o}\nabla_t\left(\nabla_t \cdot \left(\hat{z} \times \vec{E}_t\right)\right) - \hat{z} \times \vec{J}_t$$

Next, we expand these vectors in terms of the normalized electric and magnetic modes of the "empty" waveguide:

$$\vec{E}_t(x,y,z) = \sum_i V_i(z)\vec{e}_i(x,y) \qquad \vec{J}_t(x,y,z) = \sum_i \chi_i(z)\vec{e}_i(x,y)$$
$$\vec{H}_t(x,y,z) = \sum_i I_i(z)\vec{h}_i(x,y) \qquad J_z(x,y,z) = \sum_i \xi_i(z)e_{z_i}(x,y)$$

Electric field is expressed as follows:

$$\vec{E}(\vec{r}) = \int_V \overline{\overline{G}}_e(\vec{r},\vec{r}') \cdot \vec{J}(\vec{r}')dV'$$

where the electric dyadic Green's function is:

$$\begin{aligned}\overline{\overline{G}}_e(\vec{r},\vec{r}') = \sum_i \frac{-Z_i}{2}\vec{e}_i(x,y)\ \vec{e}_i^{\,*}(x',y')\exp(-j\beta_i|z-z'|) \ + \\ \sum_i \frac{-sgn(z-z')}{2}\ e_{z_i}^{TM}(x,y)\hat{z}\ \vec{e}_i^{\,TM*}(x',y')\exp(-j\beta_i|z-z'|) \ + \\ \sum_i \frac{-sgn(z-z')}{2}\ \vec{e}_i^{\,TM}(x,y)\ \hat{z}\ e_{z_i}^{TM*}(x',y')\ \exp(-j\beta_i|z-z'|) \ + \\ \sum_i \frac{-1}{2\ Z_i^{TM}}\ e_{z_i}^{TM}(x,y)e_{z_i}^{TM*}(x',y')\hat{z}\ \hat{z}\exp(-j\beta_i|z-z'|) \ + \\ \frac{-1}{j\omega\varepsilon_0}\delta(x-x')\delta(y-y')\delta(z-z')\hat{z}\ \hat{z}\end{aligned}$$

Magnetic field is expressed as follows:

$$\vec{H}(\vec{r}) = \int_V \overline{\overline{G}}_m(\vec{r},\vec{r}') \cdot \vec{J}(\vec{r}')dV'$$

where the magnetic dyadic Green's function is:

$$\begin{aligned}\overline{\overline{G}}_m(\vec{r},\vec{r}') = & \sum_i \frac{-sgn(z-z')}{2}\vec{h}_i(x,y)\ \vec{e}_i^{\,*}(x',y')\exp(-j\beta_i|z-z'|) + \\ & \sum_i \frac{-Z_i^{TE}}{2}\ h_{z_i}^{TE}(x,y)\hat{z}\ \vec{e}_i^{\,TE*}(x',y')\exp(-j\beta_i|z-z'|) + \\ & \sum_i \frac{-1}{2\ Z_i^{TM}}\ \vec{h}_i^{TM}(x,y)\ \hat{z}\ e_{z_i}^{TM*}(x',y')\ \exp(-j\beta_i|z-z'|)\end{aligned}$$

J.J.H. Wang, "Analysis of a three-dimensional arbitrarily shaped dielectric or biological body inside a rectangular waveguide", IEEE Trans. Microw. Theory Tech., vol. MTT-26, no. 7, pp. 457-462, July 1978

R&D activities

- Study of the electromagnetic energy radiated by a multipactor discharge occurring within a realistic microwave passive component: E-plane waveguide transformer implemented in WR-75 rectangular guide

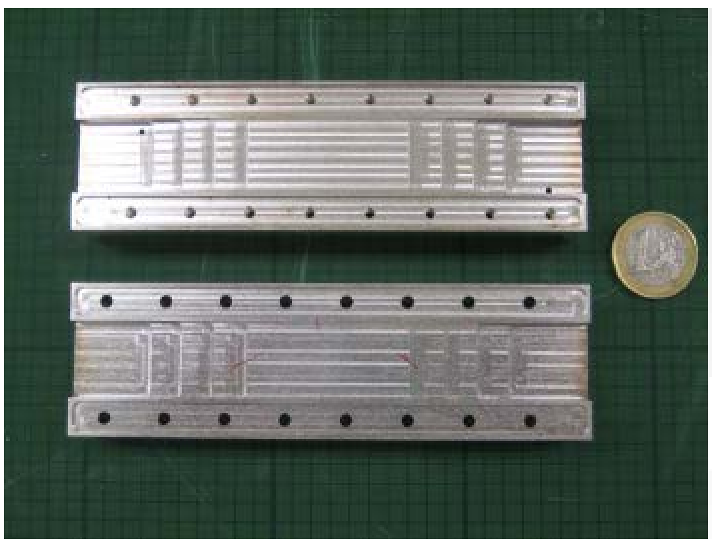

Scheme: a=19.05 mm

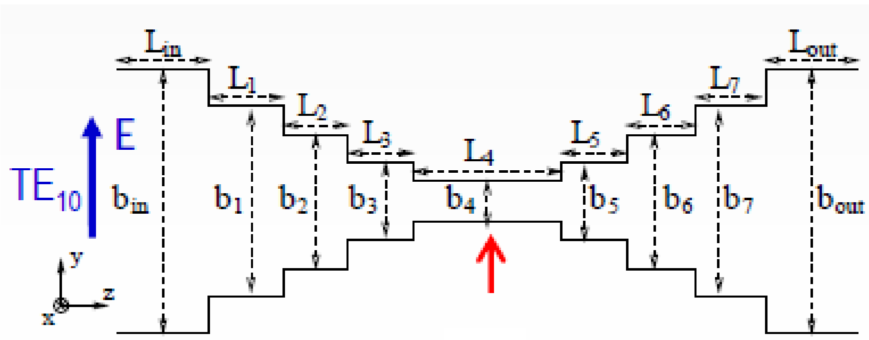

WG Section	L_i (mm)	b_i (mm)
in	20.00	9.53
1	8.11	5.46
2	8.03	1.44
3	8.24	0.44
4	40.04	0.32
5	8.24	0.44
6	8.03	1.44
7	8.11	5.46
out	20.00	9.53

Electrical response:

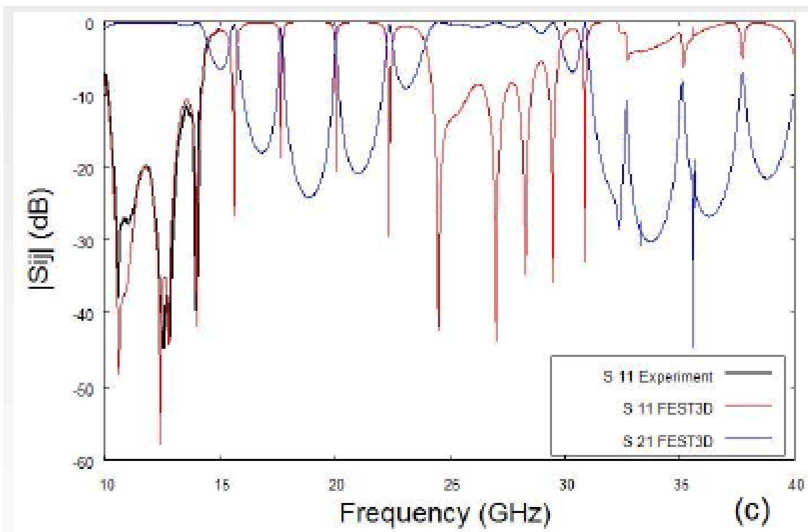

Vertical electric field pattern within the central gap:

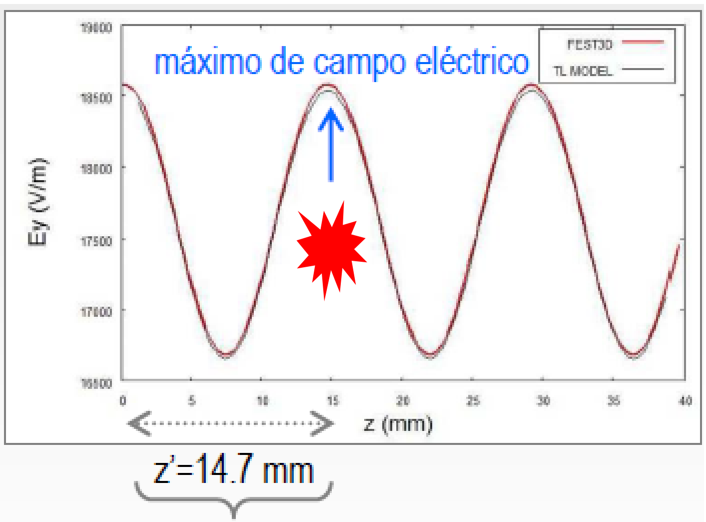

Location of the discharge

Ag; f = 12.466 GHz
d = b4 = 0.32 mm, **f x d = 3.99 GHz mm**

Multimode equivalent network representation including the multipactor discharge as a time-harmonic current source

FOURIER TRANSFORMATION

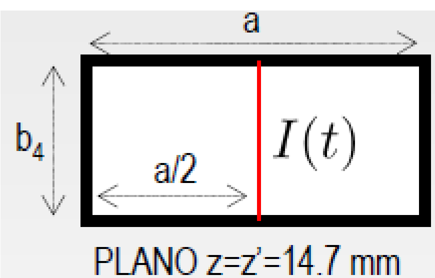

$$\boxed{I(t) = \frac{-e}{d}\, v_e(t)}$$

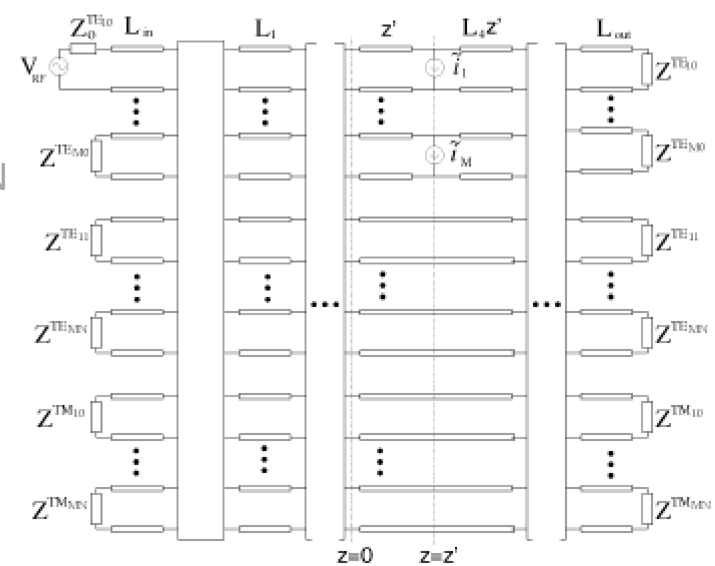

Comparison between measurements and theory is succesfull:

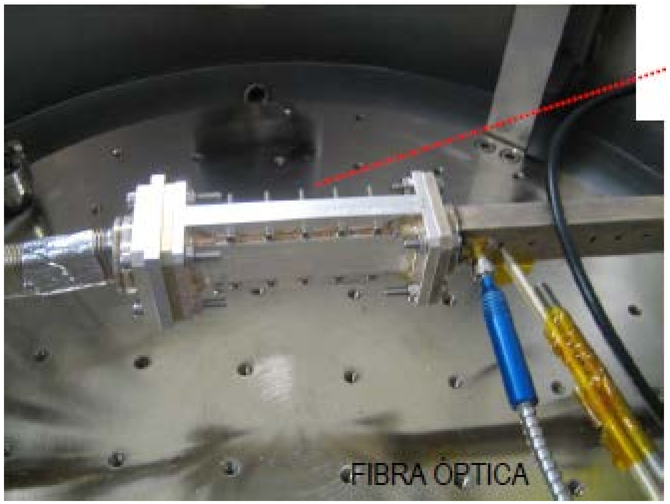

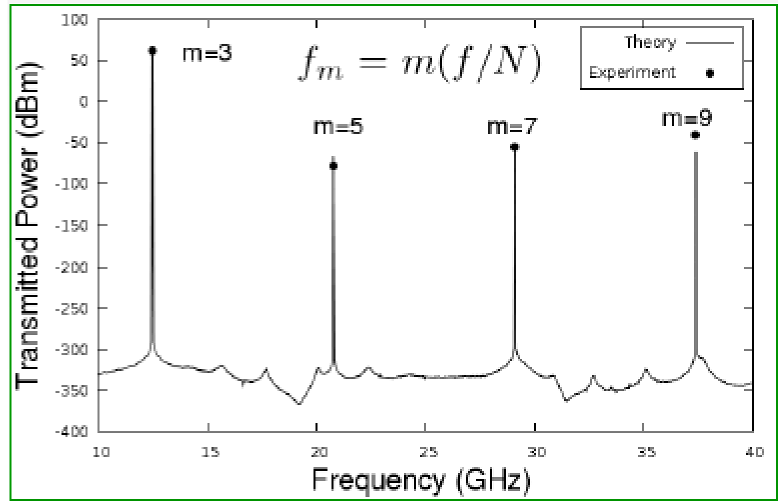

M. Jiménez, B. Gimeno, C. Miquel-Espanya, D. Raboso, S. Anza, C. Vicente, J. Gil, F. Quesada, A. Álvarez, M. Taroncher, M. Reglero, V.E. Boria, J. Phys. D: Appl. Phys. 43 (2010) 395501 (7pp)

M. Jiménez, B. Gimeno, D. Raboso, S. Anza, A. Álvarez, F. Quesada, V. E. Boria, C. Vicente, J. Gil, IEEE Microwave Wireless Components Letters, vol. 22, no. 2, pp. 61-63, Febr. 2012

- Electromagnetic fields of a charge moving with constant velocity along the axis of an arbitrarily-shaped waveguide: calculation of the weak-fields

Singular current density in time-domain:

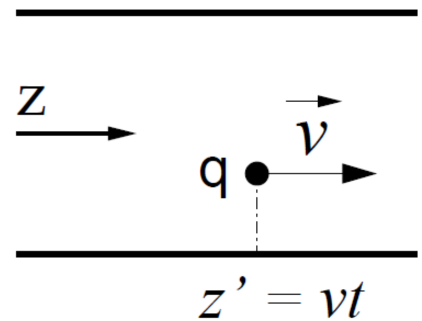

$$\rho(\mathbf{r}', t) = q\,\delta(x' - x_0)\,\delta(y' - y_0)\,\delta(z' - v\,t)$$

$$\vec{\mathcal{J}}(\mathbf{r}', t) = \rho(\mathbf{r}', t)\,v\,\hat{\mathbf{z}}$$

Fourier transformation of the singular current density:

$$\mathbf{J}(\mathbf{r}', \omega) = q\,\delta(x' - x_0)\,\delta(y' - y_0)\,e^{-i\omega\,z'/v}\,\hat{\mathbf{z}}$$

Convolution integral with the electric and magnetic dyadic Green's functions allow to calculate the frequency-domain fields:

R&D activities

$$\mathbf{E}_t(\mathbf{r},\omega) = \frac{q}{v\ \varepsilon_0}\sum_m k_{t_m}^2 \mathbf{e}_m^{TM}(\mathbf{r}_t)\Phi_m^{TM}(\mathbf{r}_0)\frac{e^{-i\,\omega\,z/v}}{\left(\frac{\omega}{v\ \gamma}\right)^2 + k_{t_m}^2} \tag{10a}$$

$$E_z(\mathbf{r},\omega) = -\frac{i\ q}{\omega\varepsilon_0}\sum_m k_{t_m}^4 \Phi_m^{TM}(\mathbf{r}_t)\Phi_m^{TM}(\mathbf{r}_0)\frac{e^{-i\,\omega\,z/v}}{\left(\frac{\omega}{v\ \gamma}\right)^2 + k_{t_m}^2} \tag{10b}$$

$$\mathbf{H}_t(\mathbf{r},\omega) = q\sum_m k_{t_m}^2 \mathbf{h}_m^{TM}(\mathbf{r}_t)\Phi_m^{TM}(\mathbf{r}_0)\frac{e^{-i\,\omega\,z/v}}{\left(\frac{\omega}{v\ \gamma}\right)^2 + k_{t_m}^2} \tag{10c}$$

$$H_z(\mathbf{r},\omega) = 0 \tag{10d}$$

Finally, time-domain fields are analytically calculated:

$$\vec{\mathcal{E}}_t(\mathbf{r},t) = \frac{q\ \gamma}{2\ \varepsilon_0}\sum_m k_{t_m}\mathbf{e}_m^{TM}(\mathbf{r}_t)\Phi_m^{TM}(\mathbf{r}_0)e^{-k_{t_m}\gamma|vt-z|} \tag{11a}$$

$$\mathcal{E}_z(\mathbf{r},t) = -\frac{q}{2\varepsilon_0}u\left(t-\frac{z}{v}\right)\cdot \sum_m k_{t_m}^2\Phi_m^{TM}(\mathbf{r}_t)\Phi_m^{TM}(\mathbf{r}_0)e^{-k_{t_m}\gamma|vt-z|} \tag{11b}$$

$$\vec{\mathcal{H}}_t(\mathbf{r},t) = \frac{q\ v\ \gamma}{2}\sum_m k_{t_m}\mathbf{h}_m^{TM}(\mathbf{r}_t)\Phi_m^{TM}(\mathbf{r}_0)e^{-k_{t_m}\gamma|vt-z|} \tag{11c}$$

$$\mathcal{H}_z(\mathbf{r},t) = 0$$

Using this definition of δ-function wake-fields:

$$\mathbf{w}_t(\mathbf{r},\mathbf{r}',s) = \frac{1}{q}\int_0^L \vec{\mathcal{E}}_t\left(\mathbf{r},t=\frac{z+s}{v}\right)dz + \\ + \frac{v\ \mu_0}{q}\int_0^L \widehat{z}\times\vec{\mathcal{H}}_t\left(\mathbf{r},t=\frac{z+s}{v}\right)dz \tag{13a}$$

$$w_z(\mathbf{r},\mathbf{r}',s) = -\frac{1}{q}\int_0^L \mathcal{E}_z\left(\mathbf{r},t=\frac{z+s}{v}\right)dz \tag{13b}$$

R&D activities

we obtain:

$$\mathbf{w}_t\,(\mathbf{r},\mathbf{r}',s) \;=\; \frac{L}{2\;\gamma\;\varepsilon_0}\sum_m k_{t_m}\,\mathbf{e}_m^{TM}(\mathbf{r}_t)\,\Phi_m^{TM}(\mathbf{r}_t')\,e^{-k_{t_m}\gamma s} \tag{14a}$$

$$w_z\,(\mathbf{r},\mathbf{r}',s) \;=\; \frac{L}{2\;\varepsilon_0}\sum_m k_{t_m}^2\,\Phi_m^{TM}(\mathbf{r}_t)\,\Phi_m^{TM}(\mathbf{r}_t')\,e^{-k_{t_m}\gamma s}$$

The following waveguides have been studied with the BI-RME (Boundary Integral - Resonant Mode Expansion) technique:

G. Conciauro, M. Bressan, and C. Zuffada, IEEE Trans. Microwave Theory Tech. **32**, 1495 (1984).
S. Cogollos, S. Marini, V. E. Boria, P. Soto, A. Vidal, H. Esteban, J. V. Morro, and B. Gimeno, IEEE Trans. Microwave Theory Tech. **51**, 2378 (2003).

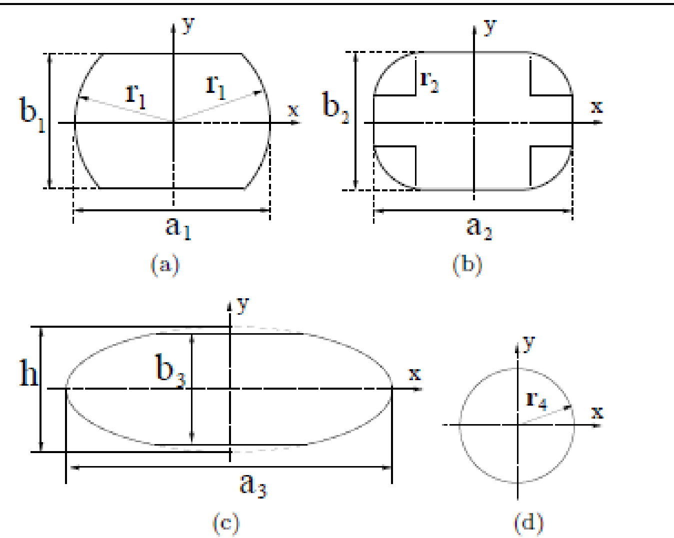

FIG. 9: Cross-section of the waveguides studied in section III B: **(a)** LHC beampipe. **(b)** Rounded-corner rectangular waveguide. **(c)** LHC beampipe modified with elliptical side walls. **(d)** Circular waveguide.

Numerical results of the δ-function axial wake-fields potentials:

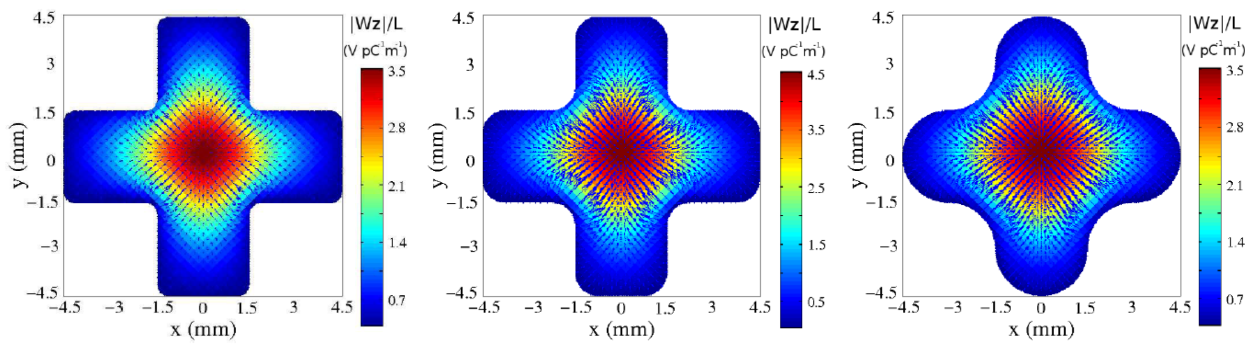

(a) (b) (c)

Figure 5. δ-function wake potential for cross-shaped waveguides with different radius of curvature. Picture of the transverse plane at a distance $s = 5\ \mu$m behind the source charge. $\mathbf{r}'_t = (0, 0)$, $\beta = 1 - 10^{-7}$. The colorbar stands for $|W_z|/L\ (V\ pC^{-1}\ m^{-1})$ and the arrows point to the direction of $\mathbf{w}_t$. **(a)** $r = a/8$, **(b)** $r = a/4$, **(c)** $r = a/2$.

More numerical results for a charge shifted:

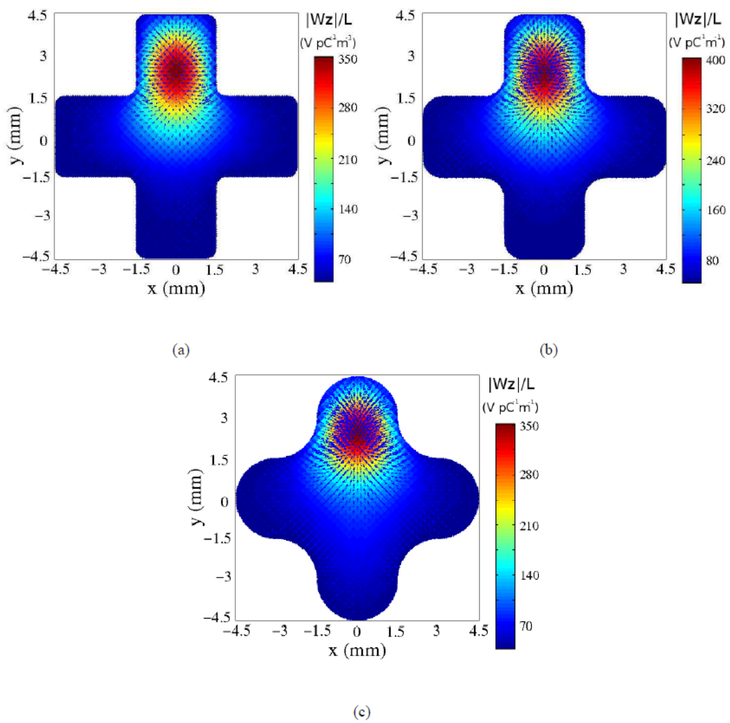

Figure 6. δ-function wake potential for cross-shaped waveguides with different radius of curvature. Picture of the transverse plane at a distance $s = 5\ \mu$m behind the source charge. $\mathbf{r}'_t = (0, 2.3)\,mm$, $\beta = 1 - 10^{-6}$. The colorbar stands for $|W_z|/L\ (V\,pC^{-1}\,m^{-1})$ and the arrows point to the direction of $\mathbf{w}_t$. **(a)** $r = a/8$, **(b)** $r = a/4$, **(c)** $r = a/2$.

Recently we have extended this formulation to deal with 3D gaussian distribution of charges:

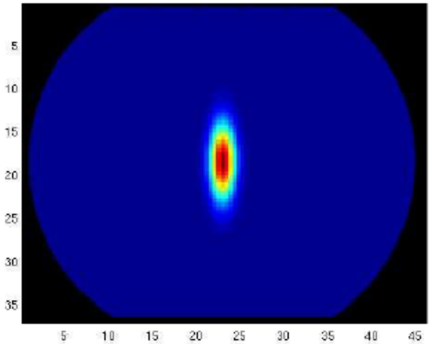

$$\vec{\mathcal{J}}^{(\text{3D-Gauss})}(\vec{r}\,',t) = \frac{Q\,v}{(2\,\pi)^{3/2}\,\sigma_x\,\sigma_y\,\sigma_z}\; e^{-\frac{1}{2}\left(\frac{x'-x_0}{\sigma_x}\right)^2}\; e^{-\frac{1}{2}\left(\frac{y'-y_0}{\sigma_y}\right)^2}\; e^{-\frac{1}{2}\left(\frac{z'-vt}{\sigma_z}\right)^2}\;\hat{z}$$

$$\vec{J}^{(\text{3D-Gauss})}(\vec{r}\,',\omega) = \frac{Q}{2\,\pi\,\sigma_x\,\sigma_y}\; e^{-\frac{1}{2}\left(\frac{x'-x_0}{\sigma_x}\right)^2}\; e^{-\frac{1}{2}\left(\frac{y'-y_0}{\sigma_y}\right)^2}\; e^{-\frac{1}{2}\left(\frac{\sigma_z\,\omega}{v}\right)^2}\; e^{-i\,\frac{\omega\,z'}{v}}\;\hat{z}$$

obtaining analytical results:

$$\vec{\mathcal{E}}_{\perp}^{(\text{3D-Gauss})}(\vec{r},t) = \frac{Q\,\gamma}{8\,\pi\,\sigma_x\,\sigma_y\,\varepsilon_0}\sum_{m=1}^{\infty} k_{t_m}\,\vec{e}_m^{\,TM}(\vec{r}_\perp)\; e^{\frac{1}{2}(k_{t_m}\,\gamma\,\sigma_z)^2}\; I_m^{TM}(x_0,y_0)$$
$$\left[\, e^{-k_{t_m}\,\gamma(z-vt)}\, erfc\left(\frac{k_{t_m}\,\gamma\,\sigma_z}{\sqrt{2}} - \frac{(z-vt)}{\sqrt{2}\,\sigma_z}\right) + \; e^{k_{t_m}\,\gamma(z-vt)}\, erfc\left(\frac{k_{t_m}\,\gamma\,\sigma_z}{\sqrt{2}} + \frac{(z-vt)}{\sqrt{2}\,\sigma_z}\right)\right] \tag{5.35a}$$

$$\vec{\mathcal{E}}_{z}^{(\text{3D-Gauss})}(\vec{r},t) = \frac{Q}{8\,\pi\,\sigma_x\,\sigma_y\,\varepsilon_0}\sum_{m=1}^{\infty} k_{t_m}^2\,\phi_m^{TM}(\vec{r}_\perp)\; e^{\frac{1}{2}(k_{t_m}\,\gamma\,\sigma_z)^2}\; I_m^{TM}(x_0,y_0)$$
$$\left[\, e^{-k_{t_m}\,\gamma(z-vt)}\, erfc\left(\frac{k_{t_m}\,\gamma\,\sigma_z}{\sqrt{2}} - \frac{(z-vt)}{\sqrt{2}\,\sigma_z}\right) - \; e^{k_{t_m}\,\gamma(z-vt)}\, erfc\left(\frac{k_{t_m}\,\gamma\,\sigma_z}{\sqrt{2}} + \frac{(z-vt)}{\sqrt{2}\,\sigma_z}\right)\right]\hat{z} \tag{5.35b}$$

where:

$$I_{\perp\perp}^{TM}(x_0, y_0) = \iint_{CS'} \phi_m^{TM}(\vec{r}_\perp{}') \; e^{-\frac{1}{2}\left(\frac{x'-x_0}{\sigma_x}\right)^2} \; e^{-\frac{1}{2}\left(\frac{y'-y_0}{\sigma_y}\right)^2} \, dCS'$$

$$erfc(x) = \frac{2}{\sqrt{\pi}} \int_x^{+\infty} e^{\tau^2} \, d\tau = 1 - erf(x)$$

INDEX

Conclusions

- The VAL SPACE CONSORTIUM has been presented as a public organisation formed by 4 public valencian entities.
- The VAL SPACE CONSORTIUM facilities have been described.
- R&D activities related with RF high-power non-linear phenomena have been reported: single-carrier multipactor effect and electromagnetic radiation.

WE ARE OPEN TO COOPERATE WITH ALL OF YOU.

The Laboratories have been co-funded with European Regional Development funds (ERDF-FEDER).

Unión Europea
Fondo Europeo de Desarrollo Regional
Una manera de hacer Europa

Thanks a lot for your attention.

Multipactor effect

- Planar circuits and transmission lines (SSPAs output sections, bridges, lange couplers, connectors, ribbons, patch antennas,…)

- **Objectives:** To investigate the effect of RF breakdown in microstrips, air-gaps, etc
- **Status:** A few theoretical studies have been performed. No simulation tools available. Need for reliable heory, simulations and experiments

TNC coaxial to microstrip transistion (LEMA/EPFL)

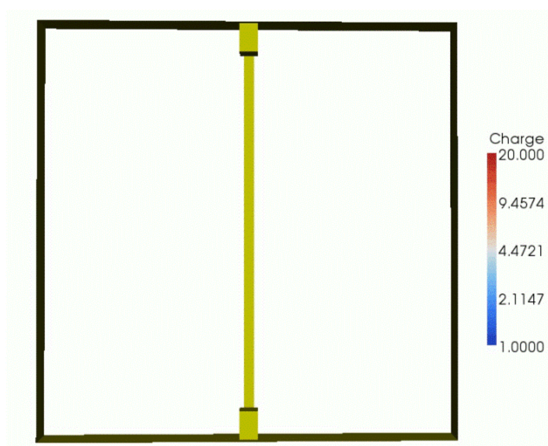

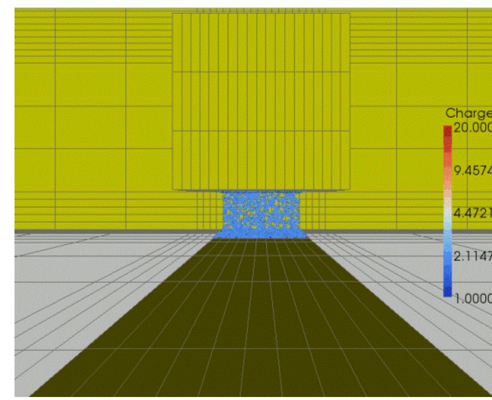

MULTIPACTOR SIMULATION IN A MICROSTRIP TO CONNECTOR

- High-power RF output sections

Theoretical modelling and validations with experimental results at laboratory

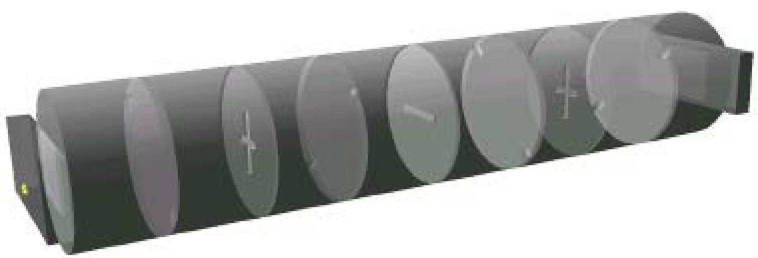

Critical central irises

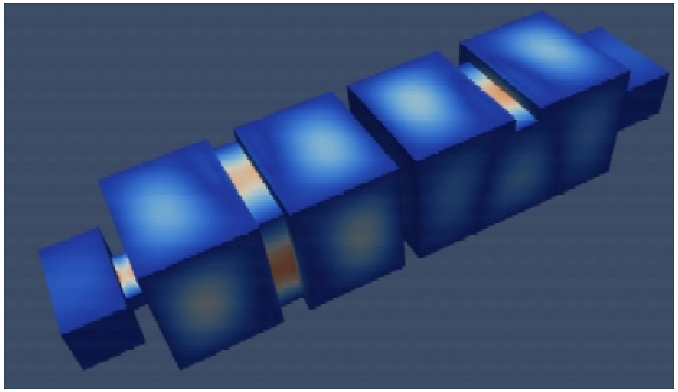

Critical input/output irises

Application to analysis of mutipactor effect considering a <u>digital modulation</u> (multi-carrier regime):

$$v(t) = V_0 \sum_{i=1}^{N} \sin\left\{ 2\pi\left[f_m + \left(i - \frac{N+1}{2} \right) \Delta f \right] t + \varphi_i \right\}$$

$\varphi_i = \varphi_i(t)$

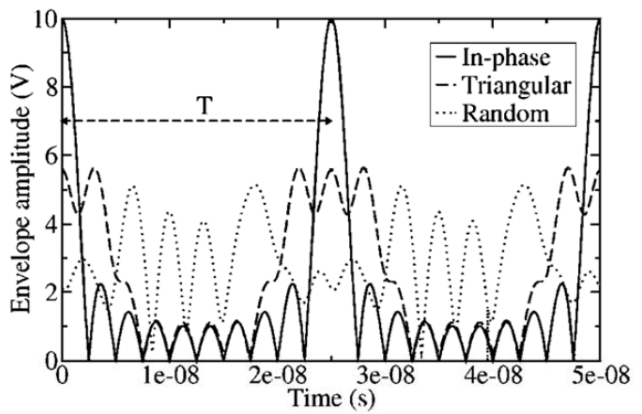

FIG. 1. Envelopes of a ten-carrier signal with a frequency separation of $\Delta f = 40$ MHz and three different phase distributions with $V_0 = 1$ V. The period is $T = 1/\Delta f = 25$ ns.

QPSK=*Quadrature* PSK

$\varphi_i = 45° \rightarrow 11$
$\varphi_i = 135° \rightarrow 01$
$\varphi_i = 225° \rightarrow 00$
$\varphi_i = 315° \rightarrow 10$

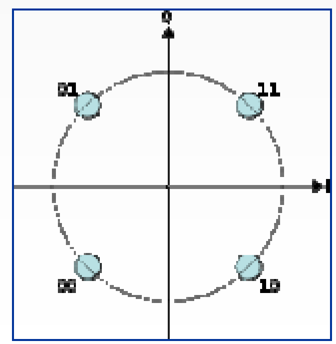

- Effect of RF breakdown in the digital modulation of an RF signal (QPSK, OFDM, etc..)

- **Objectives:** To investigate the effect of RF breakdown the BER of a telecom signal
- **Status:** Very few work available in the literature

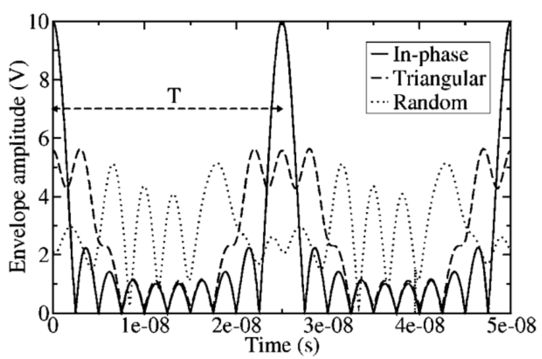

FIG. 1. Envelopes of a ten-carrier signal with a frequency separation of $\Delta f = 40$ MHz and three different phase distributions with $V_0 = 1$ V. The period is $T = 1/\Delta f = 25$ ns.

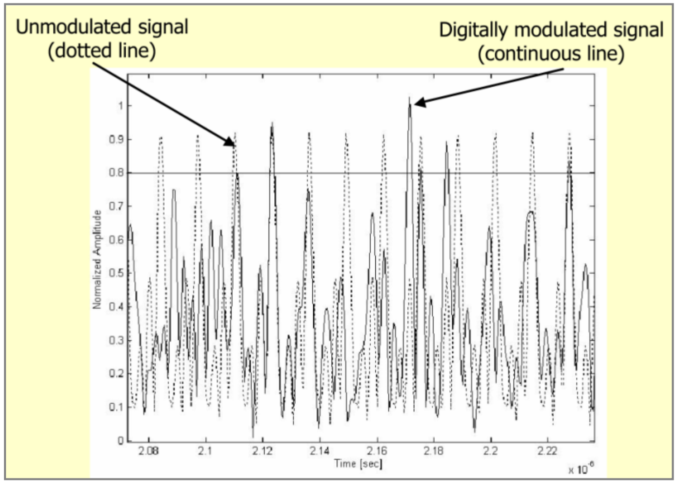

• Modulated and multicarrier signals

- **Objectives:** To investigate the effect of RF breakdown in multicarrier operation and in particular the 20 gap rule, modulated cases, phases shemes etc …
- **Technical limitations:** The lack of information in multicarrier operation implies expensive and complicate test campaigns. A rule to be used in software simulations is needed.
- **Status:** Almost no information available. Only from AEA technology and Tesat (ESA project)

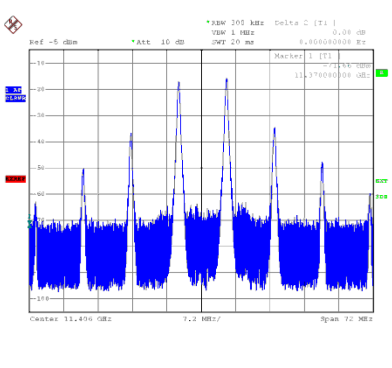

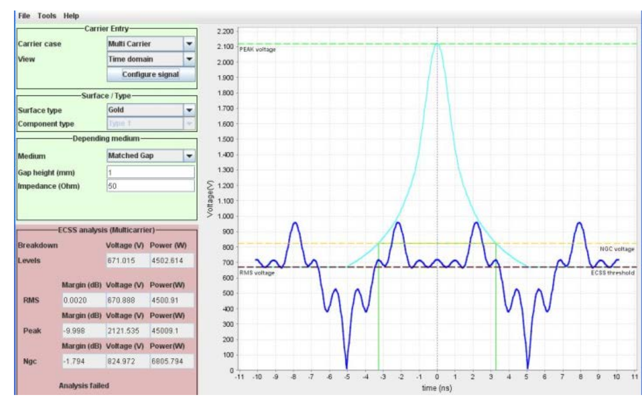

2nd tier partner program
- Main Features-

- **Objective:** associate public entities as 2^{nd} tier partners to the Laboratory's activities through at least stable financial and/or manpower support, but also through technical support and know how.
- It is also possible to get the support of European based **private satellite operators**, which have no direct financial interest in the Laboratory's activities.
- The selected 2^{nd} tier partners shall be associated to the Laboratory through **specific agreements** with VSC.
- It is ensured **equal access** to all potential European entities willing to be associated to the Laboratory's activities.

2nd tier partner program
-Other Collaborating Entities-

- **Other Collaborating Entities**:
  - **Public entities** or other European based **private satellite operators**, which have **no direct financial** interest in the Laboratory's activities.
  - This modality may allow **trainee, researchers or students** to be detached to the Laboratory for a limited amount of time.
  - Other Collaborating Entities shall be associated to the Laboratory through specific **agreements** with VSC.
  - Those Other Collaborating Entities may become at a **latter stage** 2nd tier partners by providing stable financial and/or manpower support to the Joint Laboratory